Student thesis series INES nr 572

Geometric comparison of 3D city models for daylight simulations

Johannes Lande Nyborg

2022
Department of
Physical Geography and Ecosystem Science
Lund University
Sölvegatan 12
S-223 62 Lund
Sweden

Johannes Lande Nyborg (2022)
Geometric comparison of 3D city models for daylight simulations
Master degree thesis, 30 credits in *Geomatics*
Department of Physical Geography and Ecosystem Science, Lund University

Level: Master of Science (MSc)

Course duration: *January* 2022 until *June* 2022

Disclaimer

Geometric comparison of 3D city models for daylight simulations

---

Johannes Lande Nyborg

Master thesis, 30 credits, in *Geomatics*

Supervisors:

Lars Harrie
Dep. of Physical Geography and Ecosystem Science, Lund University

Karolina Pantazatou
Dep. of Physical Geography and Ecosystem Science, Lund University

Exam committee:

Rachid Oucheikh
Dep. of Physical Geography and Ecosystem Science, Lund University

Acknowledgement

First and foremost, I want to thank my supervisors, Lars Harrie and Karolina Pantazatou. Their excellent feedback and guidance have been instrumental in developing this master thesis.

I want to thank Lund municipality for letting me use their 3D city model. Huge thanks to Hongchao Fan and Gefei Kong from The Norwegian University of Science and Technology for providing me with the VGI3D 3D city model. I also want to show gratitude to those working at DTCC Chalmers for their 3D city model and for all the assistance they have given in analysing their model.

Finally, I want to thank FME for their student licence, Lantmätriet for their Gtrans tool, and the creators of CityJSON for their CityJSON Converter tool.

Abstract

As cities keep densifying, essential resources such as daylight access become increasingly restricted. Therefore, prioritizing energy efficiency and enhancing the energy performance of our buildings is required for obtaining a sustainable urban environment. The challenges of implementing these ideas have triggered efforts to make cities smarter, for example, by using 3D city models for solar energy and daylight access simulations. While 3D model daylight simulations can help carry out planning duties, planners have been hesitant to employ them due to the difficulty of data integration and the time required to prepare input data and set up the models.

In this thesis, three different 3D city models are geometrically compared and utilized to estimate daylight access in buildings. The reference model is Lund municipality's official 3D city model. The two models compared to the reference model are VGI3D, created by researchers from NTNU, Norway, and DTCC, created by a research team at Chalmers University, Sweden. The comparisons are based on spatial accuracy, geometry, level of detail, and spatial resolution. The daylight metric used is obstruction angle, which is calculated to determine how much skylight reaches the interior of a building or apartment. In an attempt to make daylight simulations more accessible, an open-source GIS tool was designed, implemented, and published to automate the calculation of obstruction angles using 3D window information and a digital surface model.

The obstruction angles were affected the most by differences in geometry and the level of detail of surrounding buildings, usually due to differences in height. Spatial accuracy and spatial resolution did not seem to influence the results much. The comparison results showed that the accuracy of the 3D city models varied. VGI3D's results were, for the most part, relatively accurate. However, it did have one outlier in both geometry and spatial accuracy. Chalmers' results were very accurate for geometry and spatial accuracy, with two exceptions related to the height of the buildings caused by uncertainties in the input data.

Keywords: *Geography, Physical Geography, Ecosystem Analysis, 3D city model, 3D building models, daylight access, daylight simulations, obstruction angle, free and open-source software, sustainable urban development*

Abbreviations

2D - Two-dimensional

3CIM - 3D City Information Modeling, Cooperation project between Stockholm, Gothenburg, and Malmö municipality, and Lund University

3D - Three-dimensional

ADE - Application domain extension

API - Application programming interface

BIM - Building information model

CAD - Computer-aided design

CityGML - City Geography Markup Language

CityJSON - City JavaScript Object Notation

DEM - Digital elevation model

DSM - Digital surface model

DTCC – Digital Twin Cities Centre - Chalmers

FME - Feature Manipulation Engine, Software for integrating spatial data

GIS - Geographic information system

GUI – Graphical user interface

GML - Geographic markup language

ISO - International organization for standardization

JSON - JavaScript Object Notation

LoD - Level of detail OGC - Open geospatial consortium

VGI - Volunteered geographic information

VGI3D - Volunteered geographic information platform for 3D building models

XML - Extensible markup language

Table of Contents

1. Introduction

1.1 Background

There is an ongoing migration of people from rural to urban regions worldwide. United Nations (2018) predicts that approximately 68% of the world's population will be living in cities by 2050, from 55% in 2018. As a result, cities are being densified to accommodate the growing demand for housing and services. Densification poses health issues to the city's inhabitants (Pierce & Andersson, 2017) and leads to conflicts regarding essential resources such as space-use efficiency and daylight access (Dogan & Knutins, 2018). Additionally, cities are one of the most significant drivers of climate change due to their major contribution to greenhouse gas emissions (European Commission, n.d.). Cities consume more than two-thirds of the world's energy and generate more than 70% of global CO_2 emissions (United Nations, 2020). A swift transition to energy efficiency in urban settings is critical, especially for the building stock, which accounts for most urban energy use (European Commission, 2020). In the EU, almost 75% of the building stock is energy inefficient (European Commission, 2019). City governments, energy suppliers, housing businesses, and private property owners must unite and mobilize around a shared low-carbon urban energy policy (Nouvel et al., 2015).

When cities become denser, sustainable urban development becomes more and more valuable. Sustainable urban development entails the development of resource-efficient systems and goods and environmentally friendly solutions (Haaland & van den Bosch, 2015; Næss, Saglie, & Richardson, 2020). The European Union recognized the need for sustainable urban development and created a legislative framework to support it. It is structured by two directives: the Energy Performance of Buildings Directive 2010/31/EU (EPBD) and the Energy Efficiency Directive 2012/27/EU. These directives' main ideas are rooted in the European Green Deal (European Commission, n.d.), where prioritizing energy efficiency, enhancing the energy performance of our buildings, and generating power mainly on renewable energy sources are all critical goals.

Significant challenges such as urbanization and climate change have triggered efforts to make cities smarter (Pierce & Andersson, 2017). A way to make cities smarter is by increasing the focus on solar energy (SE) and daylight access. SE is one of the most environmentally friendly energy sources and an effective way to improve energy efficiency in buildings (Tsalikis & Martinopoulos, 2015). Furthermore, SE and daylight access are critical in shifting to sustainable cities since they affect our health and well-being, on-site renewable energy generation, economic activity, and social engagement (Kanters, Gentile, & Bernardo, 2021). Ultimately, one of the essential strategies for reaching Zero-Energy and Zero-Carbon Buildings is to design solar renewable energy sources (Jakica, 2017). As a result, emphasizing solar access in urban planning is integral to maintaining that everyone living and working in cities and communities has equal opportunities (Kanters et al., 2021).

GIS-based solar maps are one method of assessing the potential of the current built environment by displaying yearly solar irradiation on building surfaces (Theodoridou, Karteris, Mallinis, Papadopoulos, & Hegger, 2012). Solar maps are limited to 2D data (footprint geometry and DEM), which means information regarding the solar energy that affects the facade and interior

of buildings is not given. Getting this type of information, which is often crucial for engineers, architects, and urban planners requires 3D models (Jakica, 2017). Before, 3D models were mainly used for visualization, but they are currently also used for analysis, urban planning, and decision making. New national standards for building information management are now called to accommodate these additional requirements of 3D city models (H. Eriksson et al., 2020). The 3CIM project[1], a collaboration between the three largest cities in Sweden and Lund University, aims at creating a Swedish national information model based on an international 3D city model standard. One of the purposes of 3CIM is that municipalities and other actors should adapt it to assist the entire information management process.

Digital twin cities are a recent concept to develop digital duplicates of city infrastructure through 3D city models. Twin cities are linked to real-time city data and improve city monitoring, control, and decision-making through increased visualization and interaction with city data (Mohammadi & Taylor, 2017). Capturing and incorporating urban complexities across time and space makes digital twin cities valuable for evaluating urban energy management (Francisco, Mohammadi, & Taylor, 2020). One major initiative for digital twin cities in Sweden is *Digital Twin City Centre* (DTCC), coordinated by Chalmers, Gothenburg[2]. One central direction for the DTCC models is simulations (e.g., air pollution, wind, and noise). This thesis utilises a 3D city model provided by DTCC.

In this master thesis, 3D city models are utilized to estimate daylight access in buildings. The daylight metric that is chosen for this estimation is obstruction angle. The obstruction angle gives information on how high the sun must be in the sky to enter through a window of a building. A high obstruction angle means little daylight enters the building, which is often the case in urban environments. Obstruction angle is a daylight metric that can be used in the early stages of the urban planning process as it requires no information on the interior of the building. It can help provide an early or preliminary indication of adequate/or not access to daylight. 3D city models help estimate the obstruction angle by storing the buildings' window information and geometry.

1.2 Problem statement

While 3D models help carry out planning duties, planners have been hesitant to employ them due to the difficulty of data integration and the capacity to represent a sizeable 3D environment (Ahmed & Sekar, 2015). Historically 3D city models have been too computationally demanding to be a realistic option for everyone. However, in recent years, improved computing capacity, particularly GPU-accelerated processes, has enabled major advancements in solar design and light simulation, including real-time performance feedback (Jakica, 2017). Even with improved processing power accessible, calculating daylight performance indicators at a city scale remains challenging because of the work required to tailor the geographic data and set up the model (Dogan & Knutins, 2018). To fulfil the minimal criteria posed by the legal framework for urban design and management, urban planners, architects, landscape architects, and daylight experts

[1] https://www.smartbuilt.se/

[2] https://dtcc.chalmers.se/

often have to spend substantial time preparing input data for daylight simulations of various daylight metrics.

Accordingly, one of the primary drawbacks of creating 3D models today is that the users need specialized knowledge in the field (Agius, Sabri, & Kalantari, 2018). Thus highlighting the need for workflows that can automatically generate urban daylight models based on GIS data (Dogan & Knutins, 2018).

In the case of calculating obstruction angle for multiple windows, potentially in different buildings, using CAD software will likely be tedious and require expert knowledge. The user must manually find the inputs (windows and obstruction objects) before doing the calculations, meaning the software itself does not find the obstruction objects. Before this thesis, there was no GIS software available with easy-to-use workflows for automating this process, to the author's knowledge.

1.3 Aim

This master thesis aims to define a workflow including recommendations to assist anyone in using 3D city modelling tools to create solar energy and daylight access simulations in urban settings. This aim is achieved by creating a daylight access tool and comparing the accuracy, geometry, spatial resolution, and obstruction angle of three different 3D city models. The compared 3D models are developed by various organizations using their own methods.

The research questions for this thesis project are as follows:

- How should an easy-to-use workflow using GIS software be developed to calculate the obstruction angle of windows in 3D city models to help planners, architects, landscape architects, and daylight experts?
- How will different positional accuracy, geometry, level of detail (LoD), and spatial resolution of 3D building data affect the results of the obstruction angle simulations?

1.4 Limitations

There are three main limitations in this master thesis:

- The study area of this master thesis is limited to a small area of Lund for time and computational efficiency purposes. Furthermore, only a select few buildings are chosen for comparison within this study area.
- Although 3D city models can depict almost any physical object, this master thesis is limited to objects representing 3D buildings and general variation in the landscape (hills and slopes). Vegetation is not included because it is not a part of the obstruction angle metric and the 3D city models compared in this thesis do not include it.
- This thesis focuses on the input data, workflow, and comparisons of these. It does not detail the creation of the data and simulation programs/processes themselves.

1.5 Disposition

After the introduction, this master thesis is split into five more chapters.

Chapter two includes the theoretical framework, which presents essential principles for understanding the methodologies. It covers national and international standards for city models.

Additionally, examples of previous, relevant studies are also given. The third chapter describes the methodology. Chapter four presents the results of comparing three unique 3D city models and the daylight simulations. The fifth chapter includes a critical discussion regarding the implications of the results from the previous chapter. Furthermore, the limitations of the design and implementation and shortcomings of the workflow are debated. The sixth and final chapter summarises the conclusions related to the stated research questions.

2. Theoretical Framework and Standards of 3D City Models

The first part introduces the broader terms relevant to this thesis, such as sustainable urban development and solar access. Afterwards, essential elements in the technical framework that builds 3D city models are described.

2.1 Sustainable urban development

Daly (1974) established the concept of "steady-state economics", in which the economy is considered a subsystem of a closed, finite environment. A "steady-state economy" does not drain or pollute the environment beyond its regenerative and absorptive capacity, but rather strives to balance it (Daly, 1974). All modern sustainability theories are founded on this perspective of economics (Basiago, 1998). However, the theme of a "sustainable world" was coined later in the late 1970s and early 1980s by Brown, founder and president of the Worldwatch Institute. Brown addressed overpopulation, non-renewable energy sources, and the harm done to natural systems by industries (Basiago, 1998). In 1980, the United Nations Environment Programme (UNEP) and the International Union for the Conservation of Nature (IUCN) published the World Conservation Strategy, which included the phrase "sustainable development" for the first time. Sustainable development is based upon the definition of conservation: "the management of human use of the biosphere so that it may yield the greatest *sustainable* benefit to present generations while maintaining its potential to meet the needs and aspirations of future generations" (Basiago, 1998; Gilpin, 1980).

Although the overall quantity of urban areas covers a small fraction of the Earth's geographical surface, the expansion of these places is the primary cause of a variety of natural environmental concerns (Pyle, Bentzien, & Opler, 1981; Vitousek, Mooney, Lubchenco, & Melillo, 1997). Because of these negative consequences, achieving urban sustainability is one of the most important goals for urban planners and decision-makers. In terms of urban views, sustainable urban development is concerned with minor inputs of energy and resources and minimum outputs of air pollution, water pollution, and waste from an urban system. As a result, urban sustainability may also be described as increasing human quality of life within the constraints of Earth's limited resources (Pradhan, 2017). Pradhan (2017) states that urban sustainability considers three significant factors: social, economic, and environmental concerns. These factors address different parts of an urban system, such as security, livability, social fairness, improved productivity, pollution levels, and resource consumption. Sustainable urban development may be realized through efficient land use expansion and management (Pradhan, 2017). In the context of this master thesis, this can be achieved partly by employing different strategies and plans to reduce energy consumption through solar access simulations.

2.2 Solar access and solar energy

The background section of the introduction mentioned how important solar access and solar energy are for the urban environment, health-wise, and their essential factors in reaching Zero-Energy and Zero-Carbon Buildings. This section further describes and discusses these topics and how they are relevant in an urban sustainable development context.

2.2.1 Solar radiation

Solar radiation is the sun's radiant (electromagnetic) energy. The sun produces a vast amount of energy, which gives the Earth light, heat, and photosynthesis. Radiant energy is the earth's primary natural energy source, and it is needed for the environment's and its inhabitants' metabolism (Wald, 2018).

The amount of solar radiation received at a particular geographical location fluctuates over time: between day and night related to the earth's rotation and between seasons due to the earth's orbit. Regardless of the effects of clouds and other atmospheric elements, the sun and the earth's relative positions determine the solar radiation received at a particular location and time. As a result, both the sun and earth's geometry and time have a role in the amount of solar energy received at the earth's surface (Wald, 2018).

2.2.2 Solar access

What is meant by solar access in this master thesis is simply the access a physical element has to sunlight. Solar access issues generally occur when these elements are fully or partially shaded due to neighbouring structures or vegetation. Solar access and the right to light are complicated issues in any community, despite their importance to health, comfort, and happiness (Strømann-Andersen & Sattrup, 2011). The benefits of sun exposure for humans are clear: increased intake of vitamin D, better sleep, protection against type 1 diabetes, multiple sclerosis (MS), and several forms of cancer (van der Rhee, de Vries, & Coebergh, 2016; Wald, 2018; Weller, 2016).

Accelerated by the corona-pandemic, recent studies imply that buyers preferred to buy and move into houses with access to a balcony or a garden suitable for use as a home office (Hemnet, 2020; Nordlander, 2020). Good daylighting conditions have also been linked to increased productivity in the workplace and higher academic achievements in schools (Jamrozik et al., 2019). Although this may be a temporary trend, research shows that 55% to 70% of homeworkers had positive experiences working from home during the pandemic and would like to continue at least 1-3 days a week (Hamersma, Haas, & Faber, 2020). Thereupon indicating a shift towards future homes that will serve more than a residential function, furthermore resulting in an increased need for adequate solar access to homes and offices.

2.2.3 Solar energy as part of sustainable urban development

Solar radiation may be absorbed and converted into usable forms of energy such as heat and electricity through passive and active solar systems (U.S Department of Energy, n.d.). Active systems such as photovoltaic (PV) work by directly converting light into electricity (Knier, 2008), while solar thermal (ST) employs solar energy to heat a fluid (either liquid or air), which is then transferred immediately to an application or a storage device for later use (CRES, n.d.). Because cities utilize a substantial amount of energy, the deployment of PV and ST collectors in urban areas is gaining popularity. Because of their high adaptability, PV and ST systems are steadily pushing the decentralization of electricity and heat generation, making buildings practically energy independent due to a comprehensive integration of renewable energy sources (Marszal et al., 2011).

On the other hand, passive solar systems do not generate power but can help reduce a building's energy consumption. According to Cillari, Fantozzi, and Franco (2021), passive solar energy

systems may save almost 20% of a building's energy demand. Unlike active solar systems, passive solar systems do not require extra equipment. Passive solar systems are implemented purely through solar energy gained from architectural characteristics such as walls, windows, floors, and other building elements (Daneshvar Tarigh, Daneshvar Tarigh, & Nikranjbar, 2012). To accomplish a nearly zero-energy building (nZEB[3]), integrating various solutions for heat generation, cooling, and shading is critical. Such solutions can minimize building conditioning loads and maximise the percentage of energy demand supplied by renewable energy sources (Cillari, Fantozzi, & Franco, 2021).

Although solar systems are becoming increasingly popular, their technical feasibility and economic viability depend on the available solar resource. These resources are becoming increasingly scarce as cities are densifying, resulting in a lack of appropriate daylight access in buildings and outdoor settings (Iason Bournas & Dubois, 2019). Such conditions can impact our health, but they may also increase energy consumption (Strømann-Andersen & Sattrup, 2011). Because of the dynamic overshadowing effects present on building surfaces, evaluating these phenomena is critical for forecasting solar radiation availability changes, which may substantially impact solar energy usage potential (Freitas, Catita, Redweik, & Brito, 2015). Given this context, a research project of academics and industry experts was recently launched, providing scientific information to allow a reformulation of the daylight requirement in the building code based on the need for sustainable urban development (Iason Bournas & Dubois, 2019). One of the four phases of that project was a simulation-based assessment of the current building stock. As highlighted, the need for simulations in urban settings, such as daylight access, is evident (Iason Bournas & Dubois, 2019). Accordingly, supporting these simulations by giving input data recommendations for 3D city models is a part of this master thesis.

2.3 3D city models

A 3D city model is a digital representation of a city made from 3D geospatial data, including terrain, building, vegetation, transit system data, etc. (e.g., Figure 2.1). The city models, in general, are used to show, examine, analyze, and manage urban data (Döllner, Baumann, & Buchholz, 2007). Buildings are the most crucial component of a 3D city model for many purposes, but they are also the most difficult to accurately depict due to their complexity (Lancelle & Fellner, 2004). As a result, several countries have realized the necessity for a uniform representation of buildings and created national standards to define 3D building models based on their national needs (e.g., Gruber, Riecken, & Seifert, 2014; Stoter et al., 2013).

This section describes the most important elements of the 3D city models used in this master thesis. In addition, different types of relevant standards are mentioned.

[3] https://publications.jrc.ec.europa.eu/repository/handle/JRC112898

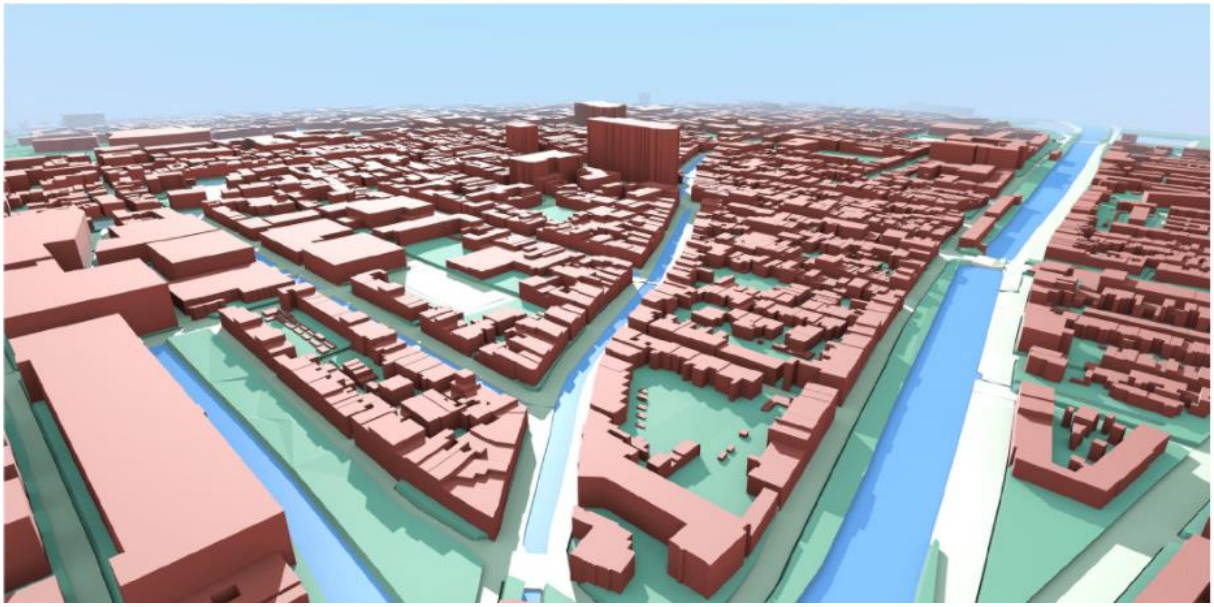

Figure 2.1: Illustration of a 3D city model. In this case, a part of the city of Delft, Netherlands, has been constructed from open-source Governmental data. Image is from Biljecki, Ohori, Ledoux, Peters, and Stoter (2016).

2.3.1 CityGML

Since 2008, CityGML has been the Open Geospatial Consortium's (OGC[4]) worldwide open standard for the representation and distribution of 3D city models. In March 2012, an expanded version 2.0 was accepted, and in 2021 OGC announced CityGML 3.0 (OGC, 2021). Aside from being an OGC standard, CityGML has received widespread acceptance in the software industry, with products from practically every prominent company providing CityGML interfaces (Gröger & Plümer, 2012).

Gröger and Plümer (2012) highlighted CityGML as one of the most widely used information models for representing objects and structures in city simulations. CityGML is a structured, open XML-based multifunctional standard for storing and exchanging data. The *Geography Markup Language (GML)* is the foundation for CityGML. The standard represents the physical representation of real-world objects and topological and semantic data (Gröger & Plümer, 2012). CityGML makes it easier to integrate urban geodata for several Smart Cities and Urban Digital Twins applications, such as urban and landscape planning, building information modelling (BIM), and disaster management, to name a few (OGC, n.d.). Furthermore, CityGML allows storing objects at various levels of detail (LoD), enhancing the ability to represent the characteristics of a city model (Gröger & Plümer, 2012).

When users gather data for an application, they frequently receive data from several sources. Sources are often collected at various periods with different techniques at varying degrees of detail and based on distinct models in terms of geometry and semantics. As a result, users confront the issue of data heterogeneity. One of the main objectives of CityGML is to solve data heterogeneity issues through standardization (Gröger & Plümer, 2012).

[4] https://www.ogc.org/

Several studies have observed poor compatibility between CityGML data and the software used to manage the data, even though city models represented in CityGML are becoming more popular (Noardo et al., 2021). Noardo et al. (2021) mention two major reasons for this. First, the geometries that describe the objects in CityGML can be represented in various ways, leaving software developers to face the challenge of developing code that deals with all possible interpretations of a single CityGML object's geometry. Second, CityGML's (hierarchical) data structure can become highly complex when data sets grow.

2.3.2 CityJSON

CityJSON is a JSON-based[5] encoding that is used to store 3D city models. CityJSON aims to provide a compact and developer-friendly format that allows files to be readily seen, processed, and altered. It was created with programmers in mind so that tools and APIs to support it may be written efficiently (CityJSON, n.d.). Data complexity should be decreased to improve interoperability and make 3D solutions accessible to a broader audience. CityJSON is a text-based data format that minimises CityGML's deep structure while maintaining the same capabilities (Ledoux et al., 2019).

CityJSON is related to CityGML by being a subset of its data model. JSON, like GML, is a text-based data interchange format that both people and machines can understand. For numerous reasons, it was chosen as an alternate encoding to GML. First and foremost, JSON dominates the web: if two types of applications need to share data, they will almost certainly utilize JSON (over XML). Second, since JSON geometry can only be stored one way, interpreting it is efficient and understandable. Thirdly, because developers widely use JSON, more libraries and applications support it, making it more likely to be maintained. Finally, JSON is built on two data structures present in almost every computer language; an ordered list of elements and objects consisting of key/value pairs (Ledoux et al., 2019). Furthermore, through bidirectional conversion between CityGML and CityJSON, it is easy to switch back and forth from one to the other (CityJSON, n.d.).

2.3.3 Level of Detail (LoD)

CityGML 2.0 features can be represented at multiple levels of detail (LoD) (Figure 2.2). With increasing LoD, the complexity of the models also increases (Gröger, Kolbe, Nagel, & Häfele, 2012). Four main characteristics define the LoD premise: First, objects of the same LoD can easily be integrated through data interoperability. Second, each level fills the requirements of different applications; therefore, it is suitable for different needs. Third, the LoDs match today's data capturing methods. Lastly, an object can be represented in multiple LoDs, allowing tools to dynamically select the most appropriate LoD for a specific task (Gröger & Plümer, 2012). Gröger and Plümer (2012) defines five different LoDs as such:

- LoD0 defines a 2.5D horizontal polygon representing a building. The polygon can either be at the height of the footprint or the roof of the building.
- LoD1 defines a building as representing a block model that can be solid or multi-surface (not entirely sealed).

[5] https://www.json.org/json-en.html

- LoD2 is similar to LoD1, except it also includes a roof structure. Furthermore, LoD2 surfaces can be split into three categories: *GroundSurface*, *WallSurface*, and *RoofSurface*. Meaning LoD2 can also be used for thematic representation.
- LoD3 is obtained by extending LoD2 with openings (windows, doors), detailed roof structures (dormers, chimneys, roof overhangs), and complex façade structures.
- LoD4 (not included in Figure 2.2) adds to LoD3 by including the buildings' interior structures.

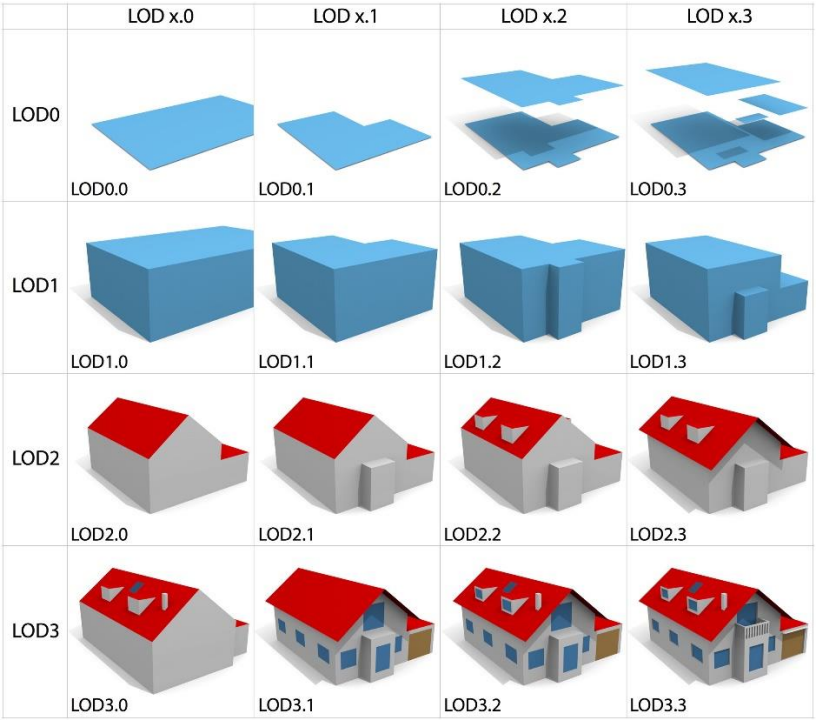

Figure 2.2: Four levels of detail in a 3D model. The image is from Biljecki, Ledoux, and Stoter (2016).

CityGML 3.0 has a slightly different LoD definition than CityGML 2.0 (Kutzner, Chaturvedi, & Kolbe, 2020). However, since this LoD definition has not been widely used yet, this master thesis adheres to the CityGML 2.0 definition.

2.3.4 Building information modelling (BIM)

Previously, blueprints and drawings conveyed information about a specific construction layout. This 2D method made visualizing dimensions and needs challenging. Then came Computer-Aided Design (CAD), which let drafters understand the value of digital blueprints. Later, CAD became 3D, increasing the realism of visualizations. Building Information Modeling (BIM) is now the industry standard. BIM is more than just a 3D model. It is a highly collaborative method that enables architects, engineers, real estate developers, contractors, manufacturers, and other construction professionals to plan, create, and build a structure or building within a single 3D model (Lorek, 2022).

BIM objects have geometry, store data, and are flexible. Flexible because BIM software automatically updates the model to reflect that change when an element is modified. Meaning all the information gathered from conception to completion is not only saved but is also actionable. Thus, keeping the model consistent throughout the procedure helps architects,

engineers, designers, and anybody part of the process to work more collaboratively (Lorek, 2022).

The most used open format to share BIM data is Industry Foundation Classes[6] (IFC), an ISO standard developed and maintained by buildingSMART[7] (buildingSMART, 2022). IFC describes a product model and data interchange format for the urban environment (Billen et al., 2014). In addition, like CityGML, IFC can store semantic information but focuses on building and structural information (buildingSMART, 2022).

2.3.5 National standards for 3D city models

Over the last decade, the popularity of 3D city models has considerably increased. Accordingly, many governmental organizations have faced challenges when introducing 3D applications into their daily processes (Stoter et al., 2013). For this reason, many countries have developed national 3D standards to assist in handling these types of problems (Gruber et al., 2014; Soon & Khoo, 2017; van den Brink, Stoter, & Zlatanova, 2013). As the accessibility of 3D city models improves, new national standards will likely continue to be developed.

The challenges governmental organizations faced regarding 3D buildings motivated Stoter et al. (2011) to create a pilot in the Netherlands to improve the use of 3D models in this country. The project's main goal was to develop a proof of concept for a 3D Spatial Data Infrastructure (SDI) by investigating the primary building components of a 3D SDI (needs, data, information, architecture, and standards), to propose a standardized 3D approach for a whole country. After the project was finished, they concluded it was a success. They highlighted that the extensive exchange of knowledge and experiences between the participants made 3D development more tangible and manageable among a broad public.

The German cadaster is a parcel-based system, which means that information is spatially related to distinct, well-defined pieces of land. The cadaster serves as the foundation for administrative, economic, and scientific duties. The buildings of each cadaster were originally only represented in 2D (Gruber et al., 2014). Gruber et al. (2014) further state that the German surveying and mapping administration recognized the need for 3D spatial information as a challenge to create and realize sustainable concepts for 3D geodata, emphasising efficient and cost-effective solutions. National and international standards, infrastructures, and activities were evaluated in this context. The German cadaster standard then incorporated ISO and OGC international standards to integrate 3D-geodata.

Another example is from Singapore (Soon & Khoo, 2017), where the Singapore Land Authority's (SLA) Land Survey Division has led a 3D mapping effort to produce and maintain a 3D national map of the country. Through airborne data collection, they made 3D models for relief, building, vegetation, and waterbodies. The project has heavily relied on the Open Geospatial Consortium's (OGC) CityGML standard (Soon & Khoo, 2017).

In Sweden, work is currently being done to implement a national standard for 3D building models (Lantmäteriet, 2022). Lantmäteriet, the Swedish mapping, cadastral, and land

[6] https://www.buildingsmart.org/standards/bsi-standards/industry-foundation-classes/
[7] https://www.buildingsmart.org/

registration authority, mentions the need for national specifications with a framework. Since they offer circumstances for several players to collaborate comparably, it also improves information flow between participants in national processes. It is one of the conditions for a national geodata platform. These specifications were partially influenced by a case study undertaken by H. Eriksson et al. (2020), the goal of which was to develop a proposal for a national building standard. The case study proposed specific requirements for the standard, such as how it should facilitate the development of 3D city models. It should connect to BIM and national registers and be based on a national categorization system for the urban environment. Based on these requirements, H. Eriksson et al. (2020) developed an Application Domain Extension (ADE) for the planned CityGML 3.0 standard building model.

2.3.6 Modeling guidelines for 3D city models

In addition to standards, guidelines are essential when gathering data, updating, and developing 3D city models. Having guidelines to follow makes it easier for individual contributors to handle geodata, which entails the improved quality of data capture, information flow, and content of 3D city models. Two examples of guides are The Modeling Guide for 3D Objects[8] – by SIG3D and Mätanvisningar (measurement instructions) by Lantmäteriet (Lantmäteriet, 2018).

The Special Interest Group 3D (SIG3D) established the Modeling Guide for 3D Objects[9] to assist users in modelling 3D objects. The guide is confined to the outer shell of buildings and is based on CityGML versions 1.0 and 2.0. The target group is developers, modellers, and data contributors. The guide mentions numerous regulations, such as overhanging building features, model structures, terrain intersection lines, heights, LoD, and reference coordinate systems, to name a few.

Mätanvisningar was developed in an earlier project denoted Swedish geoprocess. These measuring guidelines are now updated as a part of the National specifications[10] and are currently a work in progress. The guidelines state that it should be easy for various players to share geodata across administrative boundaries. Uniform geodata helps make the exercise of authority easier and more efficient in areas such as planning, property development, building permit administration, and environmental, crisis, and infrastructure projects. Geodata, including exchange formats included in this guide, are buildings (both 2D and 3D), height, waterbodies, land cover, and land use.

2.3.7 Geometry standards

Valid geometric shapes (geometric primitives) in 3D GIS datasets are often needed before they can be used in simulations (Ledoux, 2018). Still, the quality of accessible 3D datasets is often poor, with geometric and topological flaws such as duplicate vertices, missing surfaces, and self-intersecting volumes. Even though there are established international standards (e.g., ISO19107), most software manufacturers ignore them and implement simpler 3D primitives. Due to these problems, there are difficulties in reusing the datasets in other software and

[8] https://www.sig3d.eu/index.php/en/sig3d-quality-3d-city-models-qualit%C3%A4t.html
[9] https://files.sig3d.org/file/ag-qualitaet/201311_SIG3D_Modeling_Guide_for_3D_Objects_Part_1.pdf
[10] https://www.lantmateriet.se/sv/webb/smartare-samhallsbyggnadsprocess/nationella-specifikationer/

applications (Ledoux, 2018), highlighting the importance of being aware of and following international standards. ISO19107 specifies a collection of geometric primitives that, when combined, can be used to represent 3D objects. It also specifies rules for the structure of 3D primitives, which are intended to assure consistency while sharing and transforming information.

2.3.8 Quality comparison of 3D city models

Geographical data comes in various styles and combinations, with varying levels of detail and accuracy based on the nature of the data, spatial scale, capture technique, and available funding. These characteristics affect spatial analysis (Biljecki, Heuvelink, Ledoux, & Stoter, 2018). Comparing three different 3D city models from three separate organizations, as done in this master thesis, means there will be variations based on the models' methodologies and their quality of data. Therefore, it is necessary to know how they should be compared to give the fairest evaluation of each one.

Six primary components of spatial data quality are necessary to evaluate when comparing geodata (Guptill & Morrison, 2013): The first element is *lineage*, which includes information about how the source material was acquired, including all transformations. The second is *positional accuracy*, meaning how close the coordinate values of features compare to reality. The third is *attribute accuracy*, concerning how extensively and precisely the data set elements are described. Fourth is *completeness*, information about the selection criteria regarding what should be included in the data set. Fifth is *logical consistency*, the level of geometric errors, and drafting inconsistencies contained in the data set. The sixth and final element is *temporal information*, which describes the date of observation, accuracy of time calculations, type and time of update, and validity periods for spatial data records.

Errors induced by differences in LoD and positional errors from the acquisition are common concerns in 3D city models. Biljecki et al. (2018) ran an experiment to isolate and quantify these errors and determine whether the benefit of finer LoD supplied by spatial data is still applicable in circumstances of significant acquisition errors. Unlike most other experiments, Biljecki et al. (2018) used multiple error propagation analysis. They analyzed the combined effect of both LoD and positional errors, not each individually. They used the Monte Carlo method to simulate acquisition errors from a normal probability distribution in a 3D city model of multiple LoDs. Figure 2.3 illustrates two of their datasets of different LoDs overlaid on an orthophoto (LoD1 – blue and LoD2 – yellow). The data is of the same area but with different accuracy and completeness due to being produced in separate campaigns.

Figure 2.3: The illustration shows two datasets in different LoDs overlaid on an orthophoto (LoD1 – blue and LoD2 – yellow). The data is of the same area but with different accuracy and completeness due to being produced in separate campaigns. The data and the image is from Biljecki et al. (2018).

They concluded that positional error has a far greater influence than LoD. As a result, they believe that acquiring geoinformation at a fine LoD is meaningless if the collection process is inaccurate and instead recommend focusing on data quality.

2.4 Daylight simulations using 3D city models

In Sweden, urban planners rarely evaluate sunlight access to the outdoor environment and building facades or include active use of daylight (e.g., solar system) in their planning process. This is due to a lack of legislation, practice, relevant metrics, input data, and suitable tools (Kanters et al., 2021). The new European standard for daylight simulations (EN 17037:2018, SS-EN 17037:208 in Sweden) contains stricter daylight conditions regulations, such as solar access in rooms and duration of direct sunlight on specific dates.

Single building daylight simulation tools based on CAD and BIM are quite common (e.g., Jakica, 2017), but those are unsuitable for neighbourhoods or large area simulations. 2D GIS tools or 3D city models that rarely include simulations of interior daylight conditions are often used to cover multiple buildings (e.g., Figure 2.4). Another critical element to keep in mind when performing daylight simulations is the latitude of the study area. In northern countries such as Sweden, the sun angle is very low for large parts of the year, meaning shadows are long and reflectance from one building to another is important for indoor daylight.

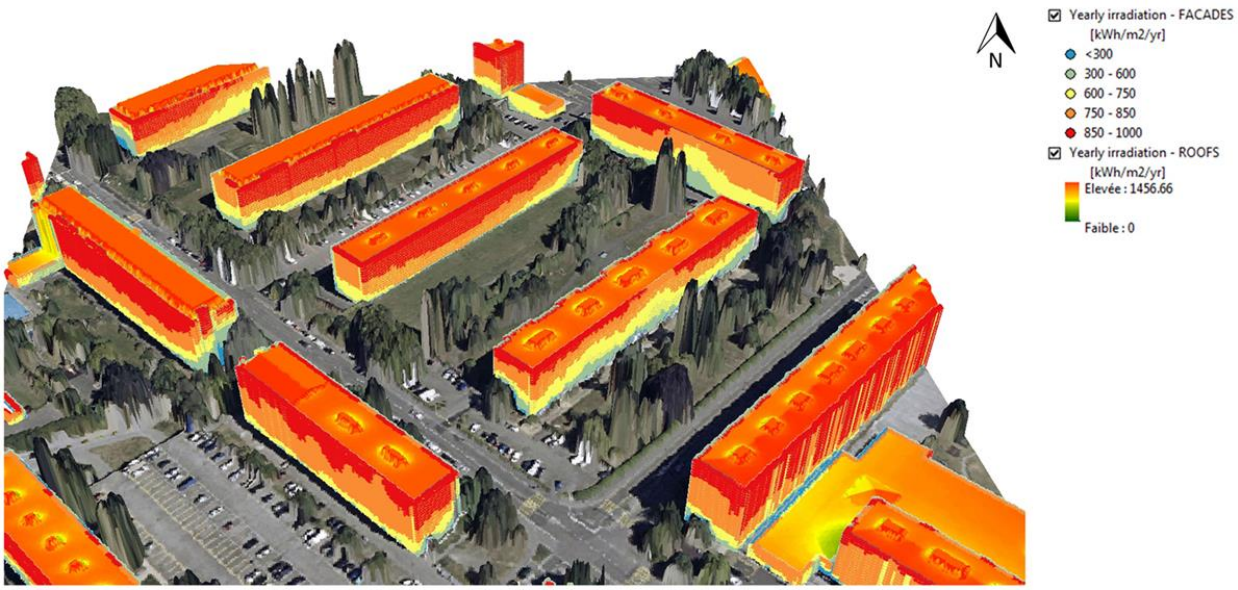

Figure 2.4: The illustration shows how 3D city models can be used for daylight and solar analysis. Here, irradiation on facades and roofs has been calculated and visually displayed on the buildings. Image is from Desthieux et al. (2018).

3D city models are appealing for daylight simulations because they may, in theory, contain all the necessary geographical information. In Sweden, most 3D city models are now in LoD2 and therefore lack crucial window information, meaning not all reflectance properties are considered (Harrie et al., 2021). For planned buildings, windows and reflectance attributes may be derived from BIM (W. Huang, Olsson, Kanters, & Harrie, 2020), and for existing buildings using street view pictures (Dogan & Knutins, 2018; Kong & Fan, 2021; Lee & Nevatia, 2004) or prior knowledge of the architectural style of the building type (Schindler & Bauer, 2003), in the context of city simulations.

Solar simulations are pretty straightforward in rural areas, where meteorological conditions affect energy yields the most (Freitas et al., 2015). The order of complexity increases in cityscapes due to limited space and three-dimensional phenomena restricting incoming sunlight. For example, urban level simulations must include the building details, a portrayal of various building types and designs, outdoor areas (open spaces, street layouts, materials, etc.), and reflectance (Freitas et al., 2015). Because of this complexity, many simulation tools are utilized simultaneously to perform the appropriate analysis (SHC, 2021). The intricacy of the urban environment creates a need to simulate local solar resources before making decisions in the planning phase, such as the installation of solar systems, placement of rooms and windows, and deciding on the height limit of new buildings in a neighbourhood.

2.4.1 Daylight metric – Obstruction Angle

A metric is a mathematical combination of measurements and/or dimensions and/or conditions expressed on a continuous scale. Therefore, we can say that daylight metrics can assess the quantity and quality of available daylight (Mardaljevic, Heschong, & Lee, 2009). The daylight metric of focus in this thesis is the obstruction angle. It is the angle between an imaginary horizontal plane through the middle of a window and the top of the object placed right in front of the window (e.g., a neighbouring building) (Swedish Standard SS914201). Alenius et al. (2019) state that the obstruction angle determines how much skylight (diffuse light) reaches the

interior of a building or apartment. For direct sunlight to enter a building, the windows must "see" the sky and the sunlight. Therefore, at a steep sun angle, the reflected light dominates in urban settings, and the availability of direct sunlight and skylight is limited (see Figure 2.5).

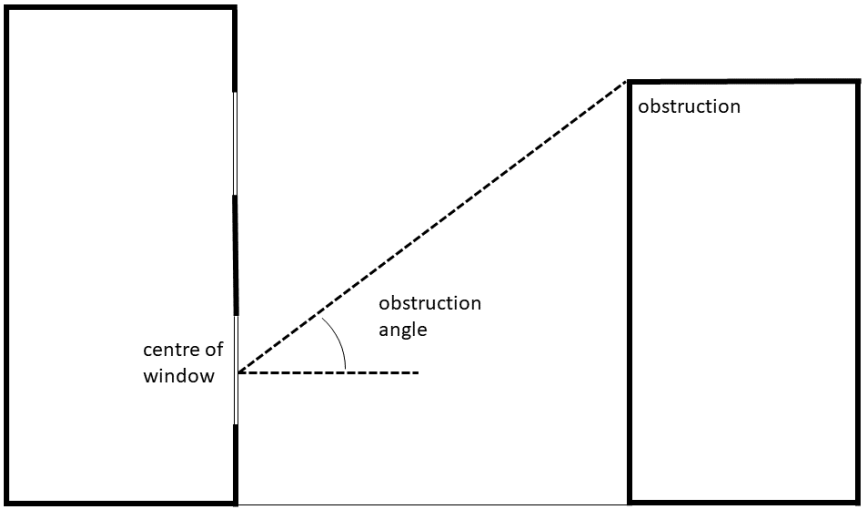

Figure 2.5: The obstruction angle metric is the angle between an imaginary horizontal plane through the middle of a window and the top of the object placed right in front of the window.

One limitation of the obstruction angle metric is that it can under or overestimate the degree of surrounding obstructions if they are not uniform (Iason Bournas, 2021), and that the window can admit more daylight around the sides of the obstruction than indicated by the obstruction angle alone (Paul Littlefair, 2001). Figure 2.6 illustrates this limitation. In this figure, you can see three different cases where all the windows will have the same obstruction angle value, yet there would be significant differences in the amount of daylight inside the rooms.

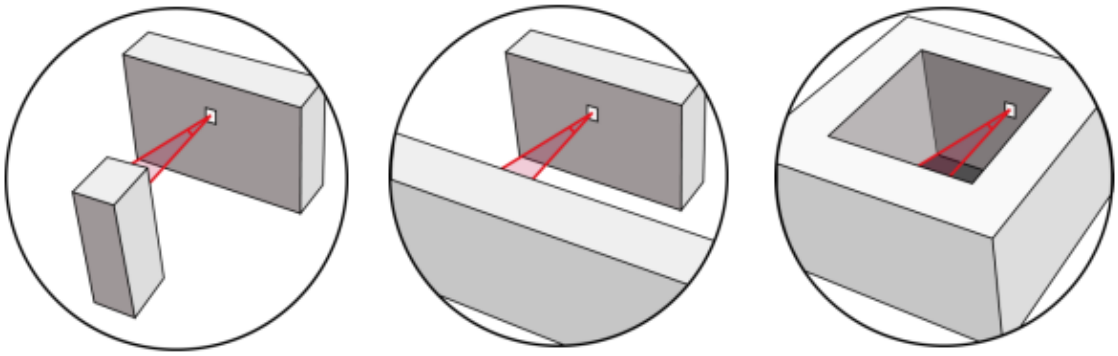

Figure 2.6: Three different situations where the obstruction angle would be the same for the windows, but the amount of daylight entering the windows would vary significantly. Image is from S. Eriksson and Waldenström (2016).

2.4.2 Methods of calculating obstruction angle in 3D city environments

Calculating the obstruction angle of a window is relatively straightforward. All you need is a window's midpoint coordinates (with z-information) and the height of an obstruction in front of it. With this information, the obstruction angle can presumably be calculated in most, if not all, CAD software. Examples of software where this can be done is with Rhinoceros[11] and Grasshopper[12] (e.g., Kanters & Davidsson, 2017), and Revit[13] (e.g., Carvalho, Alecrim,

[11] https://www.rhino3d.com/
[12] https://www.grasshopper3d.com/
[13] https://www.autodesk.com/products/revit/

Bragança, & Mateus, 2020). However, to the author's knowledge, such software does not have easy-to-use workflows for automating this process for 3D city models. That is simpler to do using GIS tools, as exemplified in this thesis.

2.4.3 Methods of comparing 3D city daylight simulations

One method to compare daylight and solar simulations for 3D city models is to simulate the same model in different LoDs. Peronato, Bonjour, Stoeckli, Rey, and Andersen (2016) did this in their research. They selected four sample buildings with varied roof shapes and elements and different types of façades. They developed these buildings in three different LoDs, 1, 2, and 3. The LoD3 building was considered the ground truth. They then calculated the total annual solar irradiation and relative error for these models. Their results indicated that coarser LoDs lead to greater potential error, mainly due to roof elements reducing or increasing the accessibility of most irradiated surfaces. Although LoD2 was not as accurate as LoD3, it is a significant improvement on LoD1 while still being suitable for largescale applications

Another example of a quality comparison of solar simulation results is the research done by I. Bournas (2020). They performed solar simulations on a sample of Swedish buildings and rooms of different geometry to evaluate which geometric measures affected the results the most. The room geometry was based on design attributes, such as room floor area, room depth, room width, glass-to-floor ratio, etc. Mann-Whitney U-tests were used to compare each geometric attribute between the two groups. The Mann-Whitney U statistic calculates the probability that a random score from one sample will be greater than a random score from a second sample. The results concluded that most of the geometric attributes had a statistically significant effect on the solar simulations.

3. Methodology

This study is a type of constructive research, meaning theories are tested, and solutions are given to problems. This thesis compares three 3D city models based on their accuracy and geometry. In addition, a tool has been developed that can automatically calculate the obstruction angle of window data in a 3D city model in combination with a digital surface model (DSM). This tool is then tested and compared for each of the three models, using DSMs in two different spatial resolutions.

All figures shown in this thesis have been created by the author, except cases where the reference is given in the figure text.

3.1 Overview

This chapter starts by describing the data and study area before it is split into five main steps, as shown in Figure 3.1. Step A involves the transformation of a 3D city model in CityGML/CityJSON format to an ArcGIS Pro compatible format, using Feature Manipulation Engine (FME). In step B the data is prepared to be analyzed by creating digital surface models for each city model. Step C deals with the comparison of the 3D city models. Step D involves the creation of a tool in ArcGIS Pro (see section 3.4 for motivation of tool) that calculates the obstruction angle of windows in the models and compares these results between each model. The final step, E, is the review, discussion, and conclusions regarding the use of tools and data.

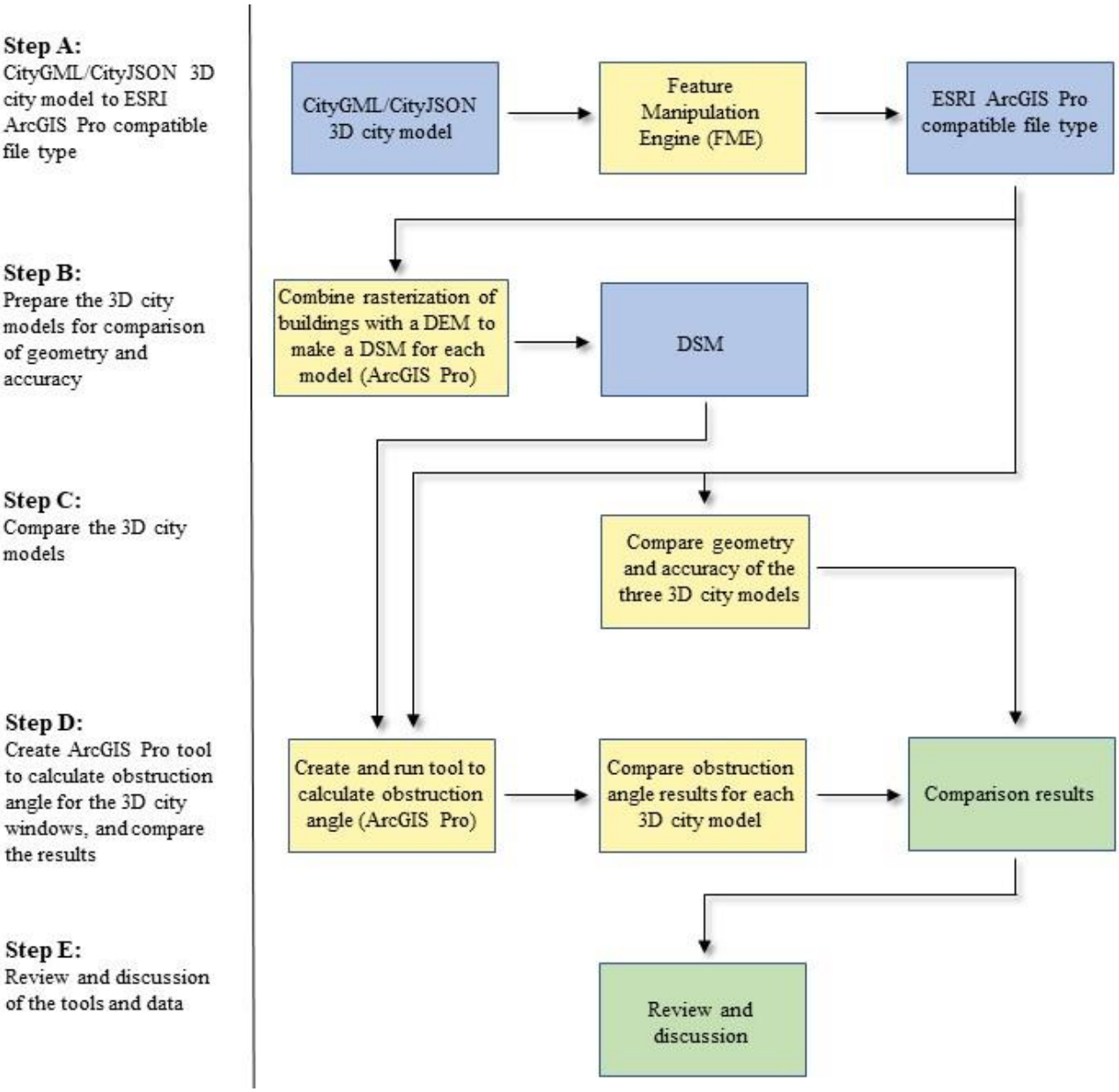

Figure 3.1: Step A to E in the figure describes the general workflow of this master thesis.

3.2 Study area

The study area is a part of Lund, a city in Skåne, Sweden. The location is in the city core, adjacent to the Central Station. The area's approximate coordinates are 55.708°N and 13.184°E.

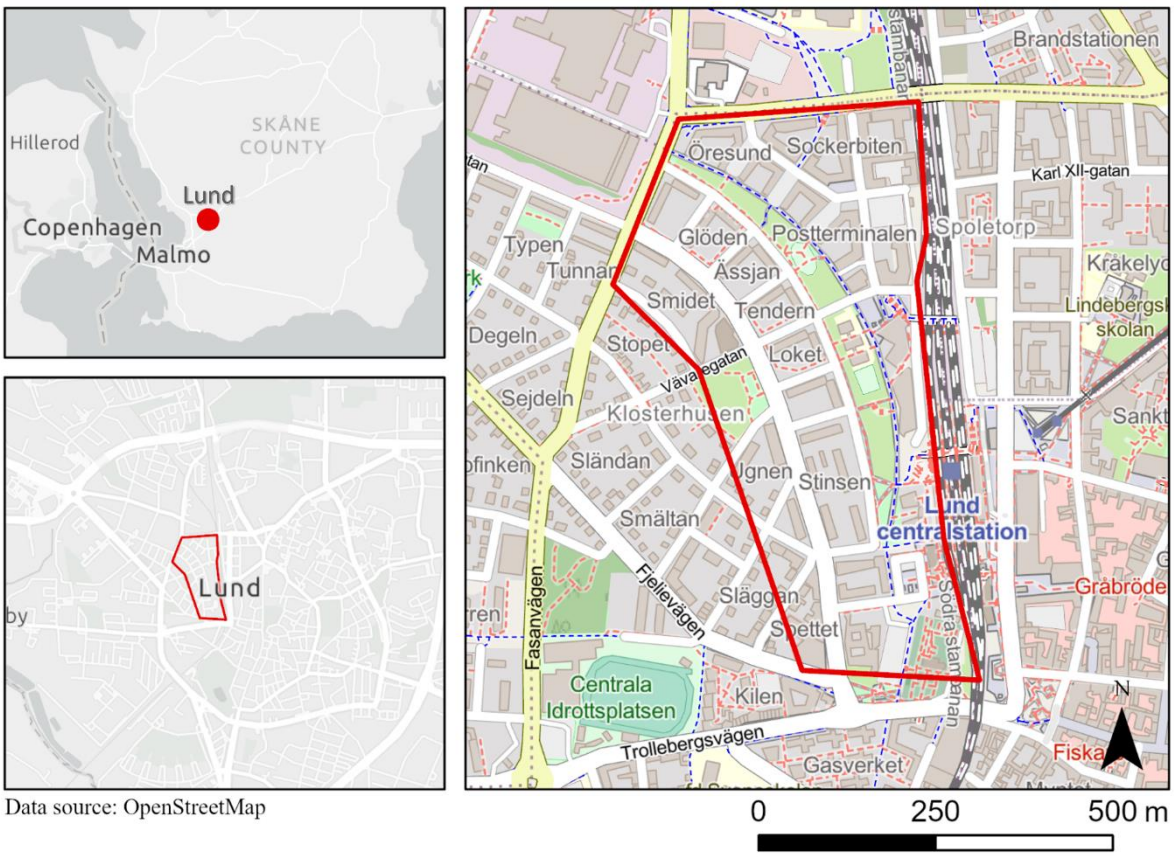

Figure 3.2: Location of the study area in Lund, Sweden.

3.3 Data

3.3.1 Digital elevation and surface models

The study area's digital elevation model (DEM) is downloaded from Lantmäteriet (product name GSD-Elevation data, Grid 2+) with a 2-meter spatial resolution. It was then resampled to 1-meter and 0.5-meter resolution in ArcGIS Pro. SWEREF 99 13 30 TM is the reference system. The dataset's positional accuracy is 0.1-meter in height and 0.3-meter in plane. The dataset is available under the FUK (Forskning, utbildning och kulturverksamhet) license.

Two digital surface models (DSM) were created for each model, one for each resolution (1 and 0.5 meters). Each DSM was created by rasterizing the buildings' roof footprints and then adding the mean DEM value for each roof footprint to this raster. Using the mean DEM values instead of the actual values for each building ensured they did not have uneven roofs. Finally, the DEM was added to the raster at all locations except at the roof footprints (workflow illustrated in Figure 3.3). The result was a unique DSM for each model, relatively close to what a real DSM would look like for these models.

Figure 3.3: An illustration of how the DSMs for each 3D city model were created.

3.3.2 3D city models

Lund Municipality

The buildings in the Lund municipality model have been generated from wire roof models from true orthophoto data (0.1 m geometric resolution). The roof models are combined with building footprints from a base map. The building footprints have either had a measured Z-value or draped on a height model. The building volumes are an intersection between a photogrammetrically measured roof model and a building area measured in the field. The wire model fully represents roof constructions on detail level LoD2. A building is split into different parts where the roof has a vertical shift of 0,50 m or more, continuous through the entire building. Buildings smaller than 12 square meters are not included.

Detailed aerial images and field measurements give this model a high level of accuracy. Additionally, the height of the buildings in the 3D city model was confirmed to be accurate by comparing them to a high-resolution DSM (0.25m) from Lantmätriet (2020). Therefore, this model is considered the true data in this thesis, which means it is used as a reference to compare the other models. It should be clear that the selection of the Lund Municipality 3D model as reference is not because it is perfect and prone of errors, but only for the sake of simple comparison.

VGI3D

Fan, Kong, and Zhang (2021) developed VGI3D, an innovative web-based interactive platform, to overcome common issues of constructing 3D models, such as high amounts of effort and time and expensive equipment. Their platform is intended to reconstruct 3D building models utilizing free photographs from internet users or the volunteered geographic information (VGI) platform, although not all these images are of great quality. With the support of a human interface module and a convolutional neural network (CNN), their interactive platform can efficiently create each 3D building model from pictures in 30 seconds. In the model used in this thesis, they used images from Google Street View and set the height of each building to 3.8 meters per storey.

Windows

3D window data is required for obstruction angle simulations. Since Fan et al.'s (2021) platform can generate window data in addition to the VGI3D city model, this was chosen as the window data that would be used in this thesis. The generation of 3D windows is based on a CNN to automatically detect the bounding boxes of windows on the facades of the analyzed buildings by combining pixel-wise segmentation and global object identification. The CNN technique delivers good results for facade parsing of windows. Google Street View photos were chosen as this thesis's street-level image data source. The georeferencing was done manually by registering relevant façade photos with their building footprint boundaries acquired from Open Street Map (OSM).

Chalmers

The information in this section is based on personal communication with Anders Logg, Vasilis Naserentin, and Dag Wästbarg from DTCC Chalmers.

The 3D city model from DTCC Chalmers is created from a set of 2D building footprints (Lantmätriet Fastighetskartan) and a corresponding 3D points cloud (a set of 3D points) from Nationella Höjdatabasen (NH). This data is available for all of Sweden through the Swedish Mapping, Cadastral, and Land Registration Authority. The height of the buildings is defined as the 90^{th} percentile of the roof Z-values (assuming there are points within the building footprint) minus the 10^{th} percentile of Z-values of the surrounding ground points. The ground is modelled only based on points classified as ground or water from the input data.

Based on the footprints, 3D points data, and a 3D bounding box, their algorithm constructs a "tetrahedral mesh of the volume defined by the intersection of the bounding box and the empty space above and between the buildings and the ground". From the tetrahedral mesh, they can also obtain a triangular surface mesh. Simply put, their algorithm relies on two main concepts. First, reducing the mesh generation from a 3D to a 2D problem. Second, solving a partial differential equation to adapt the 3D mesh to geometries of building and ground. In combination, these two ideas allow for developing a more efficient and resilient large-scale mesh from raw data. The end model is either LoD 1.2 or 1.3, depending on the quality of the input data.

The three 3D city models are shown in Figure 3.4.

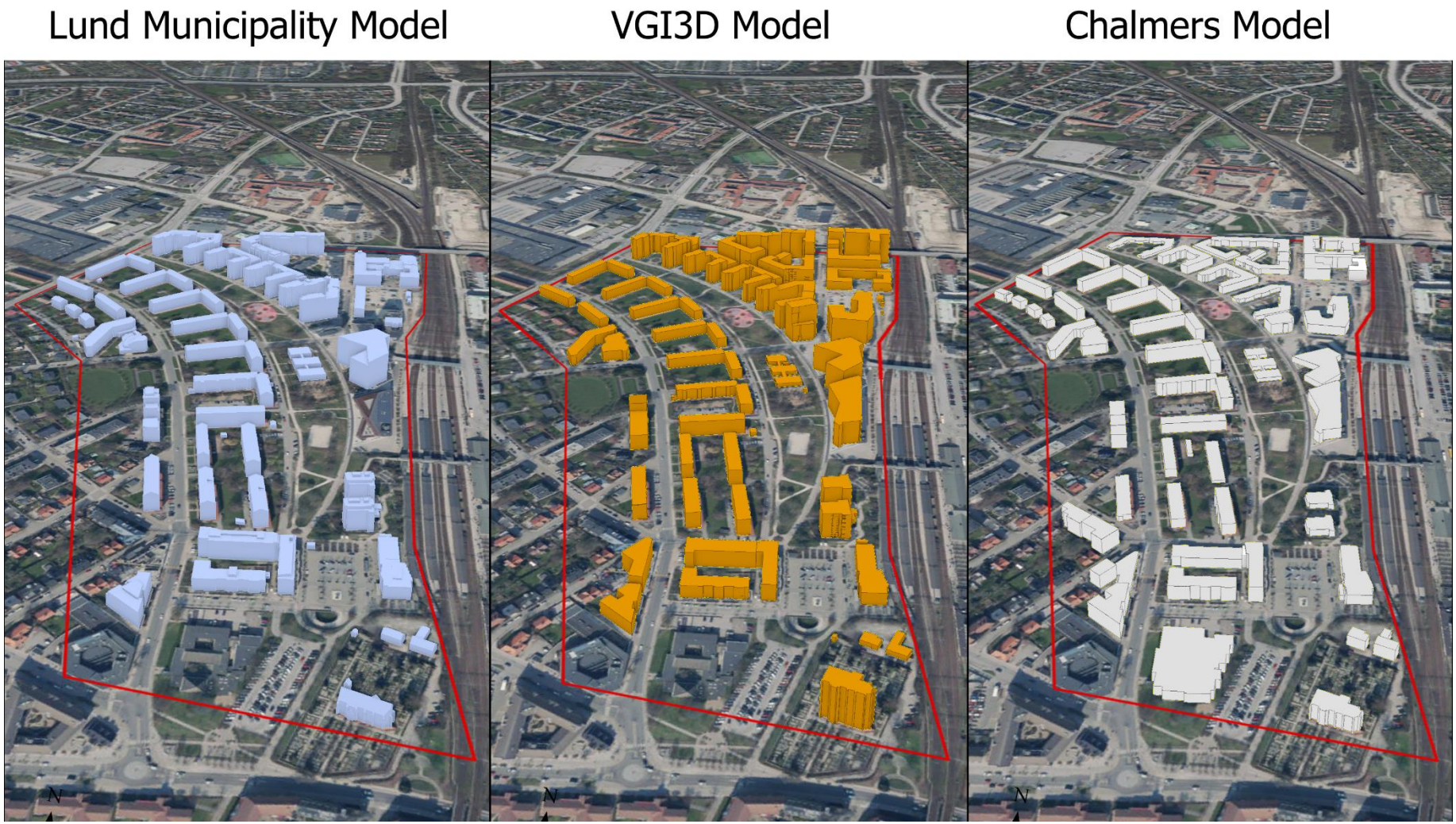

Figure 3.4: The illustration is from ArcGIS Pro and gives an overview of the three different 3D city models compared in this thesis. To the left is the Lund Municipality model, in the middle the VGI3D model, and to the right the Chalmers Model. The number of buildings vary between the models because they are made at different times.

3.4 Selection of GIS software

The GIS software of choice for this thesis is Esri ArcGIS Pro. When deciding on GIS software, the most important factor was that it could import the 3D city models and include the functionality needed to compute the obstruction angle and perform the comparison of models. Other GIS software can also do this, but ArcGIS Pro is widely used and has detailed documentation of tools and analyses. Therefore, it was chosen without investigating other software.

3.5 Transformation of file formats

The three 3D city models were all delivered in the CityJSON file format. CityJSON is not compatible with ArcGIS Pro. Therefore, it had to be transformed into another format. The obstruction angle tool was decided to only work with Esri Geodatabase (GDB) file type. For this reason, the CityJSON data was transformed to this file format. GDB was chosen for its many benefits, such as its fast performance, few size limitations, and accessible data migration, like being able to transform any other Esri Feature Class to GDB. Still, any file type compatible with ArcGIS Pro would work, but GDB was chosen because the author had intentions to use the obstruction angle tool.

The transformation of file types was accomplished by using FME. It was done by generating a workspace with a reader for the input data and a writer for the output data. When reading the CityJSON file into FME, it did not separate the city model as intended. This was because the CityJSON files I used are in version 1.0.0, while FME only supports 1.0.1 files. Although this was not an issue when importing the data in the CityGML format. Fortunately, CityJSON and CityGML are intended for bidirectional conversion, meaning changing from one to the other is easy with the official CityJSON converter[14]. When the data was successfully read to FME and the writer implemented with GDB as the output file format, the workspace was run. The only exception was the Chalmers data, which could be read as CityJSON in FME since it was stored in the appropriate version. The result was then three 3D city models that could be imported into, analyzed, and viewed in ArcGIS Pro.

3.6 Comparison of the 3D city models

Three spatial comparison analyses of the three 3D city models were chosen. The comparison is performed for six buildings in all three city models (Figure 3.5). The buildings were selected based on appearance, as the goal was to analyse six different types of buildings with different shapes and heights. Close-up images of all the compared buildings can be seen in Appendix A and B.

It is important to note that the comparison of 3D city models is not part of the research questions, where it is only asked how the models will affect the obstruction angle calculations. The goal of the comparison of these 3D models is not to evaluate them against each other or to help the reader to select one of them according to specific geometric criteria. Since the comparison is not exhaustive, it is only meant to highlight differences in these 3D models that will affect the obstruction angle computation.

[14] https://www.cityjson.org/tutorials/conversion/

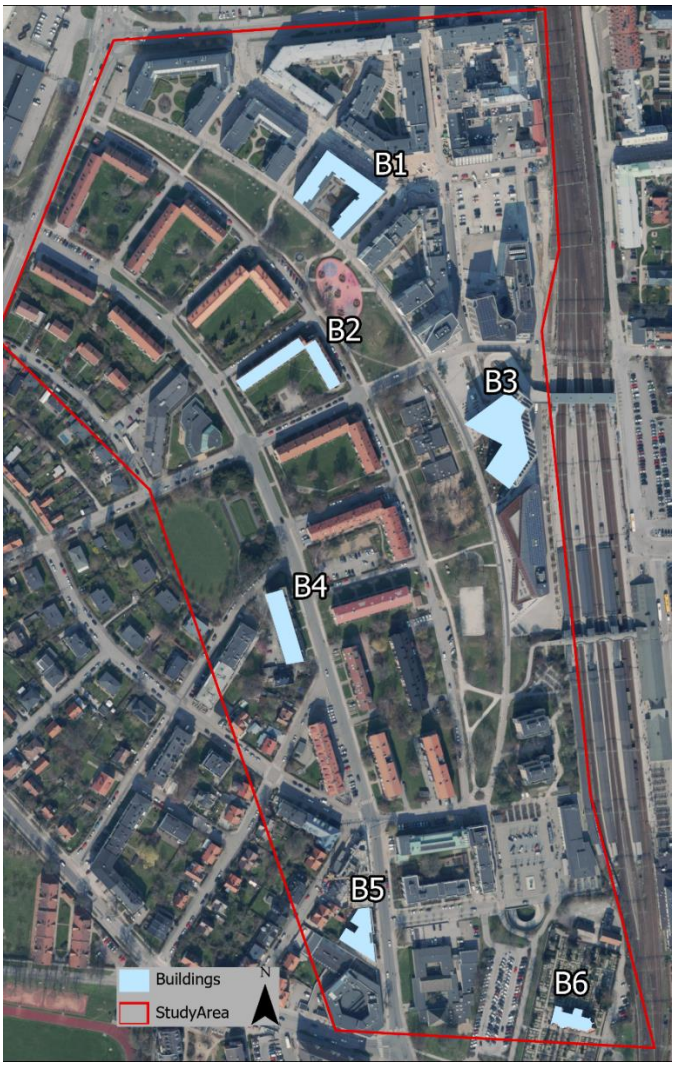

Figure 3.5: The map shows the placement of the six different buildings that have been compared based on geometry and accuracy. The blue building shapes are the footprints of the buildings from the Lund Municipality city model.

The analyses are as follows:

1. *Gross volume of individual buildings.* Accurate volume estimation of buildings is important for a variety of analyses, like urban planning (Ahmed & Sekar, 2015), population estimation (Lwin & Murayama, 2009), energy estimation (Eicker, Nouvel, Duminil, & Coors, 2014), and material estimation (Schebek et al., 2017). Volume estimation can also help measure the area of the buildings' interiors that have access to daylight.
   The volume estimation for the selected buildings was done using the *Add Z Information* tool in ArcGIS Pro. In some cases, the tool did not output a value due to the buildings not being fully closed. In those circumstances, the tool *Enclose Multipatch* had to be run on the buildings before the volume estimation.
2. *Envelope area of individual buildings.* The envelope area (the exposed building shell) may be efficiently calculated using 3D city models. This data is valuable for studying the urban heat island effect (van der Hoeven & Wandl, 2015), placement of solar systems, evaluating energy usage (Eicker et al., 2014), and other related applications.
   The building envelope was estimated the same way as the volume estimation, using the *Add Z Information* tool in ArcGIS Pro. However, this tool only lets you calculate the surface

area of the whole building, so to get the correct envelope value, the size of the footprint had to be subtracted.

3. *Positional accuracy of individual buildings.* Correct placement of buildings in a 3D city model is crucial for most simulations and city planning. In this thesis, the Lund Municipality model was used as the reference model that the two other models' positional accuracy was compared to. Absolute positional accuracy and relative positional accuracy of the building footprints are used to determine the positional accuracy of each building.
   Absolute positional accuracy is how close a measured value is to a known coordinate value in a geodetic reference system (Lund Municipality model in this thesis). The absolute positional accuracy is evaluated by comparing the difference in the coordinates of corners of the buildings in the VGI3D and Chalmers models to the Lund Municipality model. The formula used for calculating the absolute accuracy error is:

$$RMSE = \sqrt{\frac{\sum_{i=1}^{n} (X_i - x_i)^2 + (Y_i - y_i)^2}{n}}$$

   Where X and Y are the coordinates of Lund municipality, x and y are the coordinates of either VGI3D or Chalmers, and n is the number of coordinates used.
   The relative positional accuracy is evaluated by transforming (using 2D congruence (Euclidean) transformation) the VGI3D and Chalmers buildings on top of their respective buildings in the Lund Municipality models before comparing the coordinates. This transformation is performed by the tool Gtrans[15]. Congruence (Euclidean) transformation involves translation (X_0, Y_0) and rotation (α) of the coordinates, but no scale change. For the translation, the building footprints coordinates for VGI3D and Chalmers model (x, y) is translated to the Lund municipality footprint (X, Y) using the following relationship:

$$X = X_0 + x \cos \alpha - y \sin \alpha$$

$$Y = Y_0 + x \sin \alpha + y \cos \alpha$$

   where translation parameters (X_0, Y_0, α) are optimized in the least square sense to adjust the Chalmers and VGI3D footprints to the Lund municipality footprint. Once the footprints have been adjusted, the formula used to calculate the relative positional accuracy is the same as for the absolute positional accuracy.

3.7 Calculating the obstruction angles

The workflow for calculating the windows' obstruction angle (Figure 3.6) was developed by combining ArcGIS Pro tools and Python code to make an Esri Toolbox. The toolbox is publicly available on GitHub[16], where there is also a step-by-step guide on how to use it. It is released under the MIT licence.

There are two input datasets required to run the obstruction angle tool. One is 3D window data (polygons) and the second is a digital surface model (raster layer) of the area surrounding the

[15] https://www.lantmateriet.se/sv/Kartor-och-geografisk-information/gps-geodesi-och-swepos/Transformationer/gtrans/

[16] https://github.com/JohannesLN/Obstruction-Angle-Tool.git

windows. The tool starts by iterating through each window in the input dataset and then performing a set of operations on each window individually. The first operation is to find the midpoint of the input window polygons. This is calculated from the XYZ-coordinates of each vertex of the window. Next, the window midpoint, as the observation point, and the digital surface model (DSM) as the raster surface of the study area is used to run a viewshed tool. Viewshed creates a raster layer that highlights everything you can see from the observation points. From this layer, only the cells with a higher Z-value (height) than the Z-value of the window midpoint, called the obstruction points, are selected and then changed to point data. The distances and angles between the window midpoint and the obstruction points can be calculated by combining (joining) these datasets.

A viewing direction had to be calculated to find the obstruction angle of just the points opposite (perpendicular) to the window. This was done by first finding the perpendicular direction of the window. When seen in 2D, any regular window will look like a line. If this line runs from north to south (0° to 180°**)**, then the viewing direction of the window will be in the direction of east to west (90° to 270°) (Figure 3.7 gives an illustration of this). Based on this example, all the obstruction points at an angle of 90° ± 5° and 270° ± 5° within the viewshed observations would be selected. Since the tool only looks within the viewshed, it will only find obstructions away from the building. A 10° search direction range was chosen because it was relatively close to perpendicular. If there are perpendicular obstruction points for a window, then one or more of them will always be selected within this range. A smaller range could potentially "miss" the obstruction points.

The obstruction angle is then calculated for the perpendicular obstruction points, and the one with the highest value is selected as the windows obstruction angle. The value of the obstruction angle, the distance between the window and the obstruction, and the search direction are then transferred to the related window midpoint. This layer is then saved to a list before the tool iterates to the next window in the input data. Once all windows have been visited and added to the list, they are merged into one table and output.

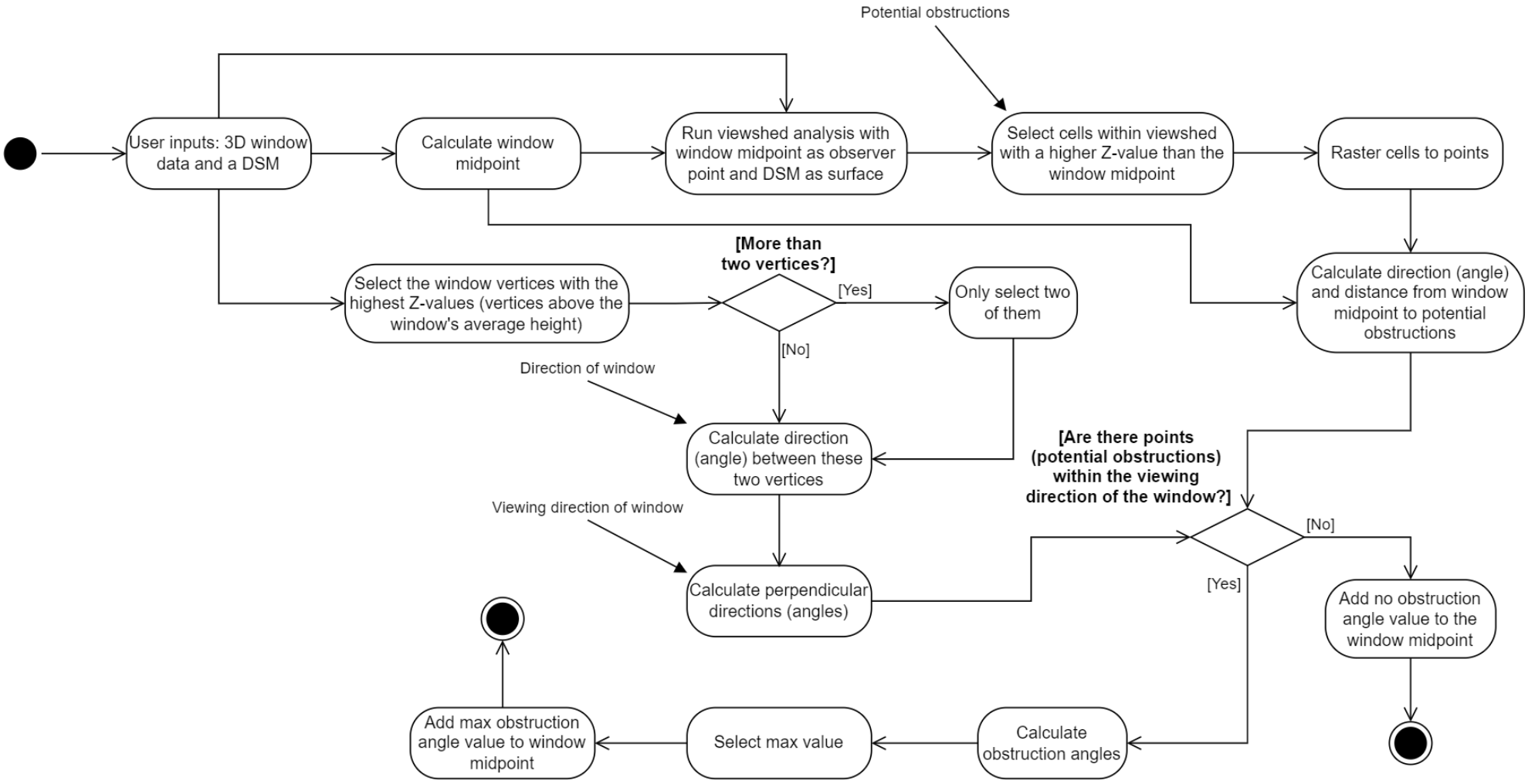

Figure 3.6: An activity UML-diagram explaining the workflow of the obstruction angle tool developed in this master thesis.

Figure 3.7 is a screenshot from ArcGIS Pro, meant to help illustrate how the tool works. The raster background is the DSM. The window is the blue rectangle. Pink points are all the obstruction points, the green points are the perpendicular obstruction points, and the single big light blue point is the perpendicular obstruction with the highest obstruction angle value. Red stippled lines are added to illustrate the viewing direction of the window. The user will only see the big light blue point's OA-value added to the window midpoint as the final output.

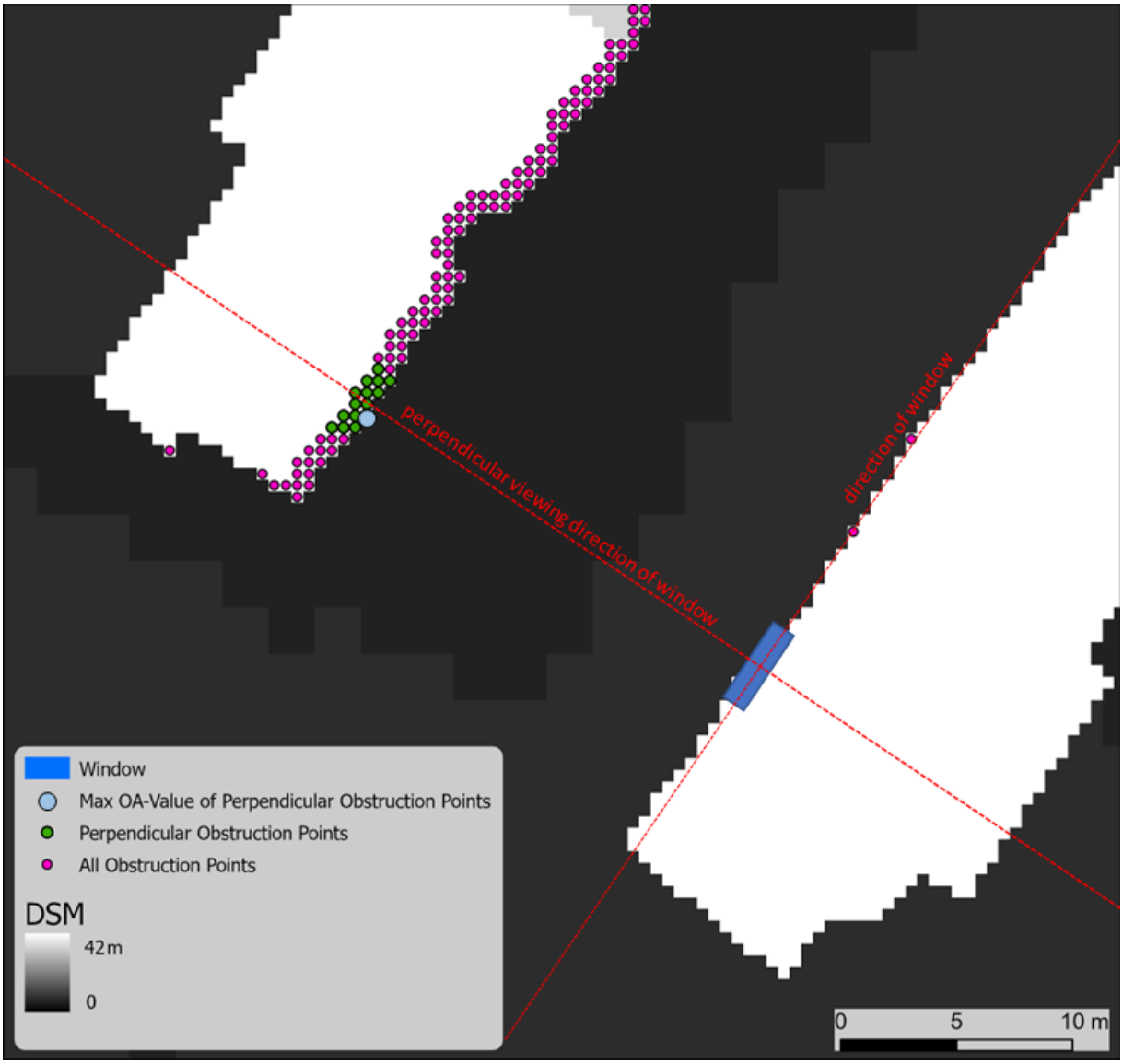

Figure 3.7: A screenshot from ArcGIS Pro to help illustrate how the Obstruction Angle Tool works. The tool finds all obstruction points (pink) and then selects only the points perpendicular to the window (points are green, and the window is blue). From the green points, the one with the highest obstruction angle value is selected (light blue) before this value is added to the window midpoint that is returned to the user. This screenshot is from the same buildings seen in Figure 3.9.

3.7.1 Running the obstruction angle tool

To run the obstruction angle tool, you first need to download the Esri ArcGIS Pro Toolbox containing the tool from GitHub[17].

[17] https://github.com/JohannesLN/Obstruction-Angle-Tool.git

Once the toolbox is downloaded and opened in ArcGIS Pro, the graphical user interface (GUI) looks like Figure 3.8. The tool requires two input data sets. One is the windows, meaning polygons with XYZ-coordinates separated as single rows in the database, representing the shape of the windows. The other required input data is a DSM of the area of interest surrounding the windows. Lastly, the tool also requires an output geodatabase folder for the output results.

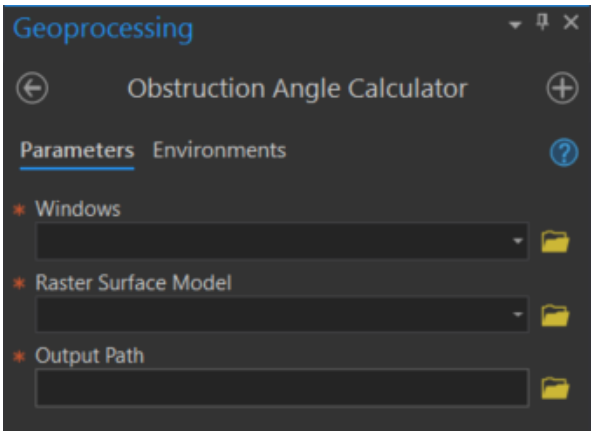

Figure 3.8: The graphical user interface of the obstruction angle tool in ArcGIS Pro

After the information has been added to the GUI and the tool is run, the output will be a point data layer where each window midpoint will have an obstruction angle value. The data visualisation can be changed in ArcGIS Pro's symbology tab. An example of how the output data can be visualized is shown in Figure 3.9. Here, using degree intervals matching the Swedish BBR-requirement[18] for daylight access.

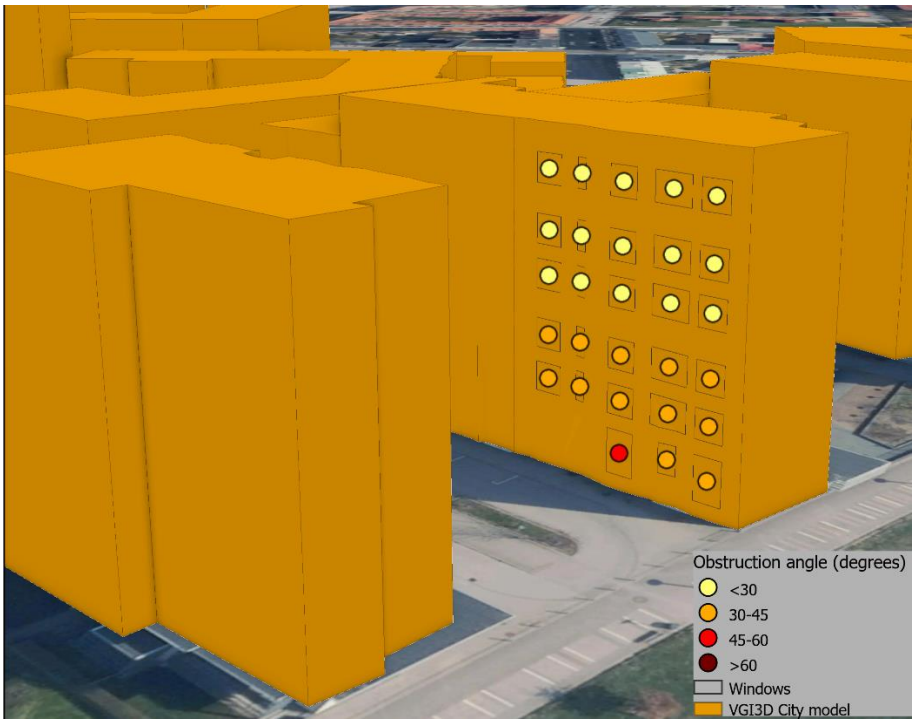

Figure 3.9: Visualization of the obstruction angle tools output on the VGI3D city model.

3.8 Comparison of the obstruction angles

To compare the obstruction angles of the three city models, the same set of window data was tested for each model. The window data was split into three window groups at separate buildings, each consisting of adjacent windows on the same façade (Figure 3.10). The groups

[18] https://www.boverket.se/sv/byggande/halsa-och-inomhusmiljo/ljussolljus/dagsljus/

contain 28, 24, and 28 windows, respectively. This number of windows was chosen as it was deemed enough to cover a large part of a façade but still not too computationally intensive. The window groups always include the lowest and highest elevation windows on the façade.

Additionally, because the city models contain a different number of buildings (see Figure 3.4), window groups were selected at locations where both models had the same selection of surrounding buildings. Window groups 1 and 2 belong to Buildings 1 and 2 (Figure 3.5). However, window group 3 is located at a building not part of the six analyzed because it was deemed a better location for the OA calculations.

It is important to note that the window data used in this thesis was originally made for the VGI3D city model (as explained in chapter 3.3.2). Hence, the windows do not fit perfectly for the Lund municipality and Chalmers city models. Therefore, the obstruction angle results are not intended to be true to reality but rather another way of comparing the three city models.

Each window group was run through the obstruction angle tool for each city model's DSM (0.5- and 1-meter resolution), meaning there were six results for each window group and 18 in total.

Figure 3.10 below shows the location and look of the three window groups.

Figure 3.10: The placement (cyan rectangles) and look of the three window groups used for the obstruction angle calculations. The VGI3D city model is the one seen in this illustration.

The results of the obstruction angle tool for each city model's DSM at both 1-meter and 0.5-meter resolution will be compared through two statistical tests:

- The difference in the maximum obstruction angle of each window group
- The mean of the difference in obstruction angle for each individual window

4. Results

In this chapter, the results of the geometric, accuracy, and obstruction angle comparisons are presented before they are discussed in the next chapter. The results are shown graphically in plots and tables and are described in the text. Visual comparisons of all buildings are shown in Appendix A and B.

4.1 3D city model result comparison

Table 4.1 summarizes all the results of volume, envelope area, absolute positional accuracy, and relative positional accuracy for the six analyzed buildings (cf. Figure 3.5) for the three 3D city models.

Table 4.1: All results for the volume, envelope area, and absolute- and relative positional accuracy for the six compared buildings.

	Building 1	Building 2	Building 3	Building 4	Building 5	Building 6
Lund Municipality						
Volume (m^3)	29316	13409	54137	13064	7852	4571
Envelope (m^2)	7286	4045	8011	3032	2383	1844
VGI3D						
Volume (m^3)	33525	11727	53070	16337	6582	12985
Envelope (m^2)	7839	3732	7825	4187	2045	3937
Absolute Accuracy (m)	0.267	0.695	0.332	2.257	0.406	0.447
Relative Accuracy (m)	0.197	0.308	0.284	1.406	0.288	0.281
Chalmers						
Volume (m^3)	12831	14464	12500	11807	7787	5256
Envelope (m^2)	3939	4402	3314	2896	2319	1810
Absolute Accuracy (m)	0.035	0.063	0.234	0.022	0.087	0.448
Relative Accuracy (m)	0.029	0.057	0.228	0.019	0.081	0.386

4.1.1 Volume

The volume of each building for the three different 3D city models is illustrated in the bar chart below (Figure 4.1).

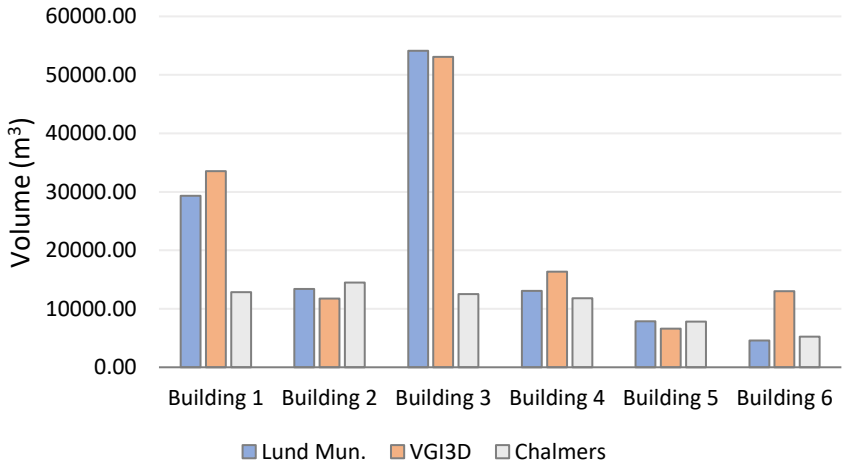

Figure 4.1: The difference in the volume of the six analyzed buildings for the three 3D city models.

The volume results show apparent differences in the size of some of the buildings. The biggest difference is found in Building 3 between Lund municipality and Chalmers, where the Chalmers

model is 333% larger (illustrated in Figure 4.3). Uncertainty in the data likely causes this massive difference, which applies to Building 1 too of the Chalmers model (discussed further in section 5.1). Buildings 1 and 3 of the Chalmers model are therefore viewed as outliers. The second biggest difference in volume is between Lund municipality and VGI3D's Building 6, where Lund's building is 184% larger (Figure 4.6). The smallest difference is found in Building 5, between Lund municipality and Chalmers, where Lund's building is only 0.8% larger (Figure 4.5). The second smallest difference is between Lund municipality and VGI3D's Building 3, where the Lund municipality model is only 2% larger (Figure 4.4).

Figure 4.2 illustrates the mean absolute difference in volume (%) of the six analyzed buildings between the Lund municipality model and the VGI3D and Chalmers city models. The figure shows the difference between all buildings (light grey) and without the two Chalmers outliers (dark grey).

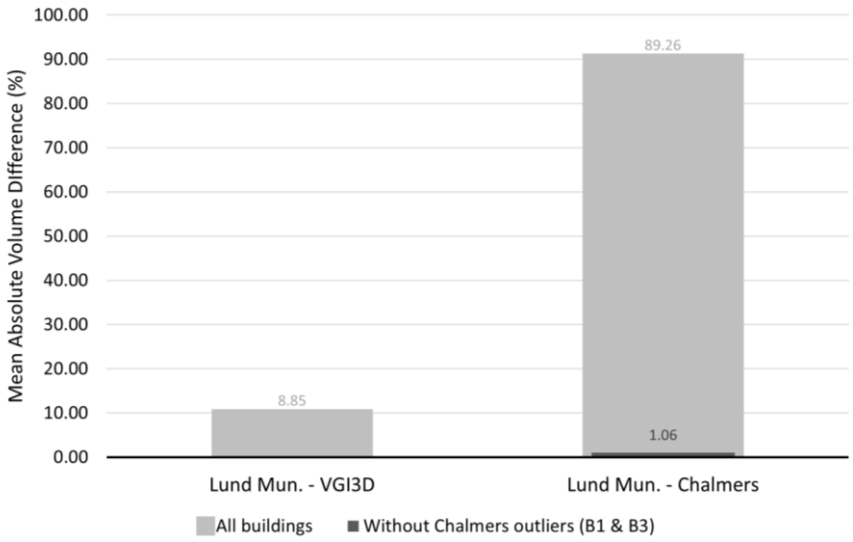

Figure 4.2: The mean absolute difference in the volume of the analyzed buildings between the Lund municipality model and the two others.

VGI3D has an 8.85% higher mean volume than Lund municipality. Whereas Lund municipality has an 89.26% higher mean volume than Chalmers when all buildings are included, if the two outliers are removed, the difference is only 1.06%.

Figures 4.3 and 4.4 illustrate the substantial difference in volume between the three models. Chalmers' Building 3, seen in Figure 4.3, has a much smaller volume than Lund municipality. Contrary, VGI3D's Building 3, as seen in Figure 4.4, has only slightly less volume than Lund's.

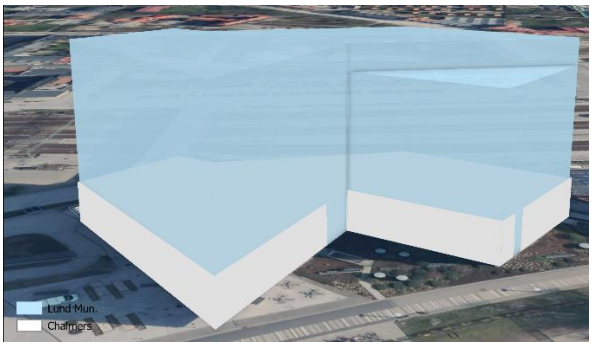

Figure 4.3: Building 3 from the Lund municipality and Chalmers models. The Chalmers building (white) has a very different volume and envelope area to Lund's, but still high positional accuracy of the footprint

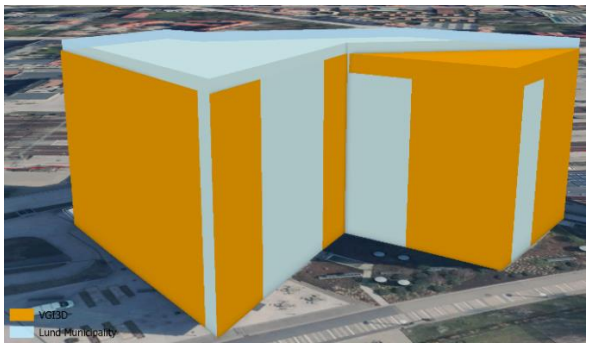

Figure 4.4: Building 3 from the Lund municipality and VGI3D models. VGI3D (orange) and Lund (blue) slightly differ in this building's positional accuracy, volume, and envelope area.

Figure 4.5 shows Building 5 of the Lund municipality and Chalmers models. These are the two buildings with the smallest difference in volume.

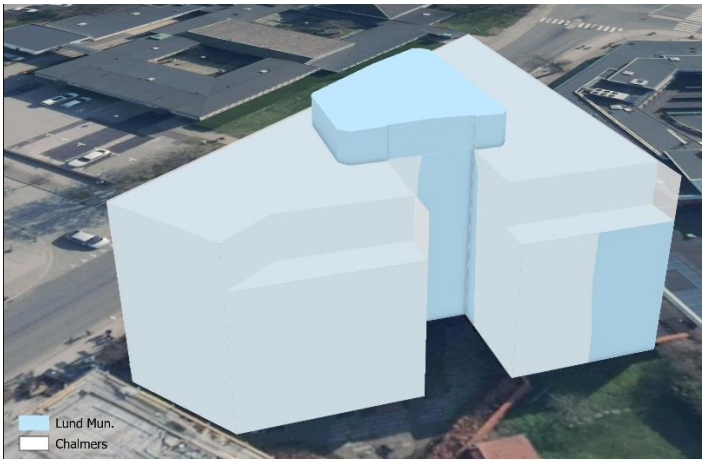

Figure 4.5: Building 5 of the Lund municipality (blue) and Chalmers (white) models. These are the buildings with the smallest difference in volume.

Figure 4.6 visualize the difference in volume for Building 6 between Lund municipality and VGI3D. These two buildings have the second-largest difference in volume of all buildings. The disparity in size for this building is likely a rare case because it has unique shapes and window geometry (discussed further in section 5.1).

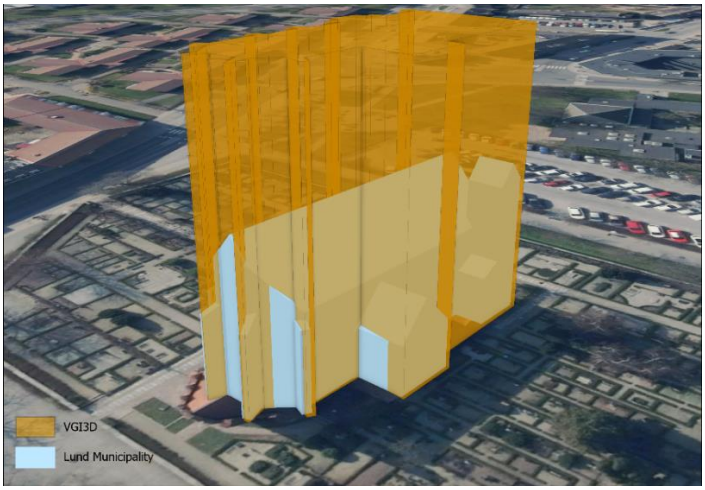

Figure 4.6: Building 6 of the VGI3D (orange) and Lund municipality (blue) models. These two buildings have the second-largest difference in volume and envelope area of any building. The substantial size difference is likely because the building has unusual shapes and window geometry.

4.1.2 Envelope area

The envelope area of each building for the three different 3D city models is illustrated in the bar chart below (Figure 4.7).

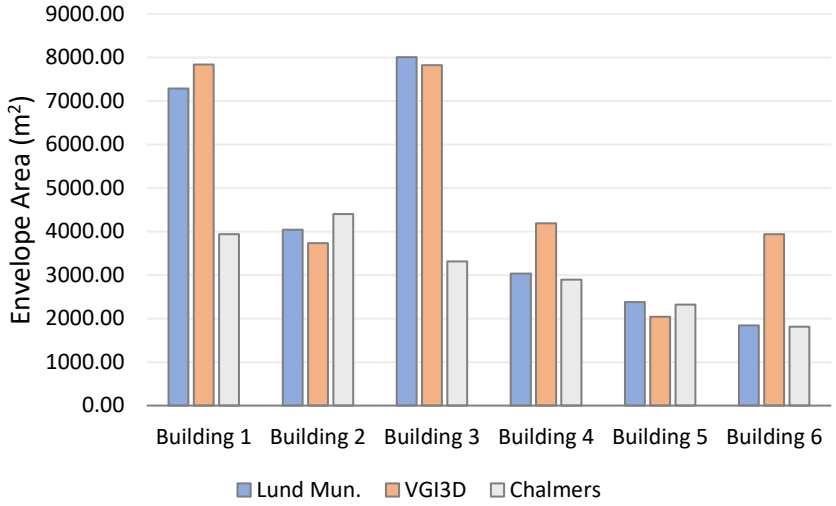

Figure 4.7: The difference in envelope area of the six analyzed buildings for the three 3D city models.

The envelope area results show considerable variations in the surface area of the buildings. Like the volume results, the biggest difference in envelope area is found in Building 3, between Lund municipality and Chalmers, where Lund's building is 142% larger (Figure 4.3). The second biggest difference is for Building 6 between VGI3D and Lund municipality, where the VGI3D model's envelope area is 113% larger (Figure 4.6). The smallest difference is found in Building 3, again between Lund municipality and VGI3D, where the Lund municipality model is only 2% larger (Figure 4.4). The second smallest is found in Building 5 when comparing Lund municipality and Chalmers, where Lund's building is 3% larger in envelope area (Figure 4.5).

Figure 4.8 illustrates the mean absolute difference in envelope area (%) of the six analyzed buildings between the Lund municipality model and the VGI3D and Chalmers city models. The figure shows the difference between all buildings included (light grey) and without the two Chalmers outliers (dark grey).

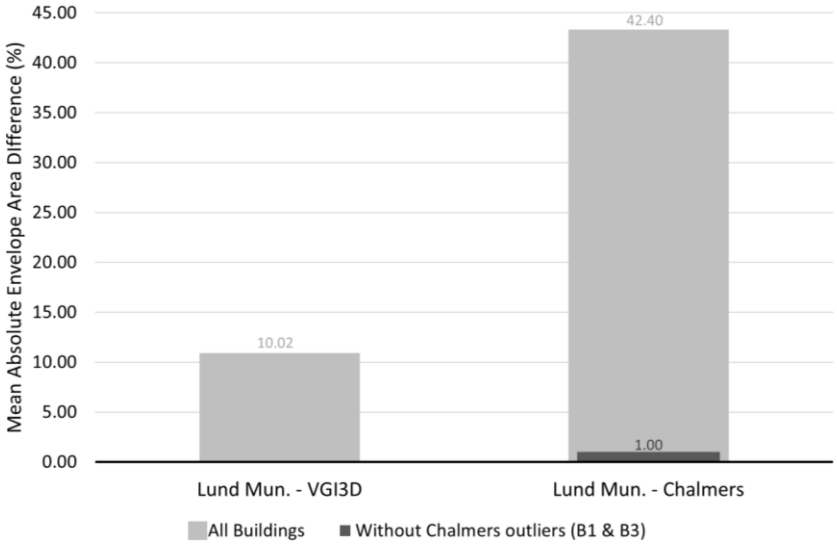

Figure 4.8: The mean absolute difference in envelope area of the analyzed buildings between the Lund municipality model and the two others.

VGI3D has a 10.02% higher mean envelope area than Lund municipality. Whereas Lund municipality has a 42.4% higher mean envelope area than Chalmers when all buildings are included, if the two outliers are removed, the difference is only 1%.

4.1.3 Absolute positional accuracy

As seen in Table 4.1 and illustrated in Figure 4.9, the VGI3D buildings have a worse absolute positional accuracy than Chalmers, except for Building 6. The best and worst relative positional accuracy is observed for Building 4, where the RMSE for VGI3D and Chalmer's model are 2.257 and 0.022 meters, respectively.

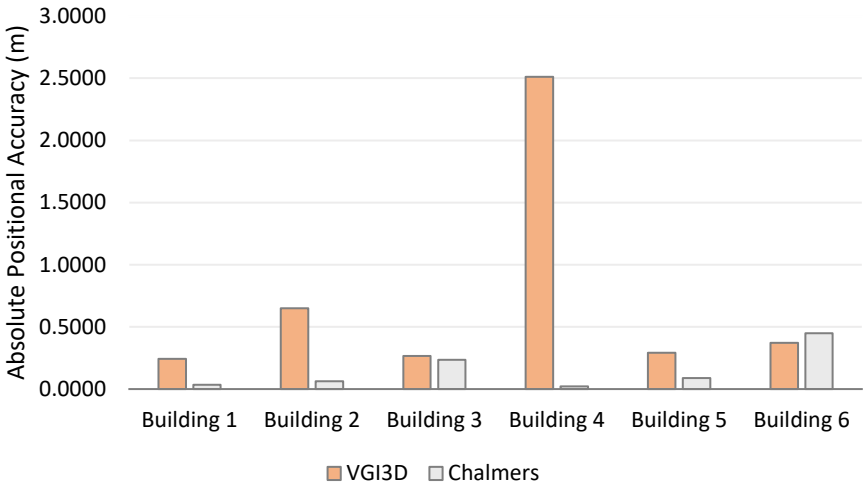

Figure 4.9: The absolute positional accuracy of each analyzed building from the VGI3D and Chalmers city models

Figure 4.10 visualize the absolute positional accuracy RMSE of VGI3D for Building 4. In this case, there is a clear difference in the footprint of the VGI3D and Lund municipality buildings. In contrast, Building 4 from the Chalmers model has the smallest absolute positional accuracy RMSE (Figure 4.11).

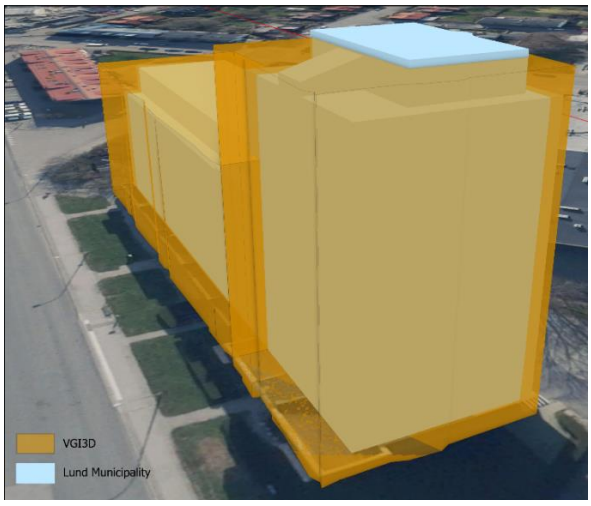

Figure 4.10: The overlayed Building 4 of the VGI3D (orange) and Lund Municipality (blue) models. This VGI3D building has the largest absolute and relative positional accuracy RMSE.

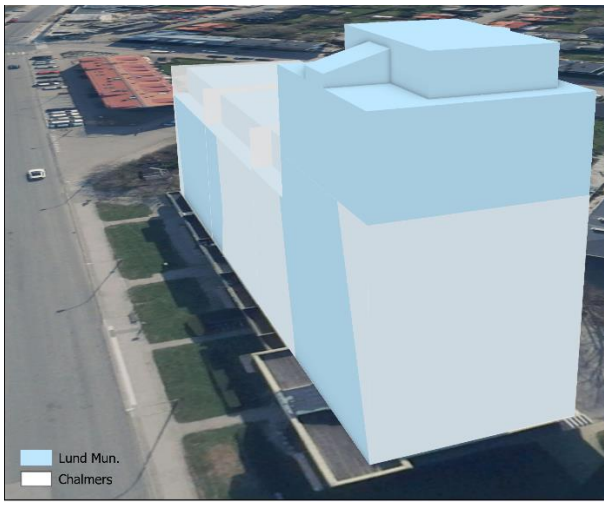

Figure 4.11: The overlayed Building 4 of the Chalmers (white) and Lund Municipality (blue) models. This Chalmers building has the smallest absolute and relative positional accuracy RMSE.

4.1.4 Relative positional accuracy

As seen in Table 4.1 and illustrated in Figure 4.12, the VGI3D buildings have a higher error of relative positional accuracy than Chalmers, except for Building 6. Like the absolute positional error, the largest and smallest error in relative positional accuracy is observed for Building 4 (Figure 4.10 and 4.11), where the RMSE for VGI3D and Chalmer's model are 1.406 and 0.019 meters, respectively.

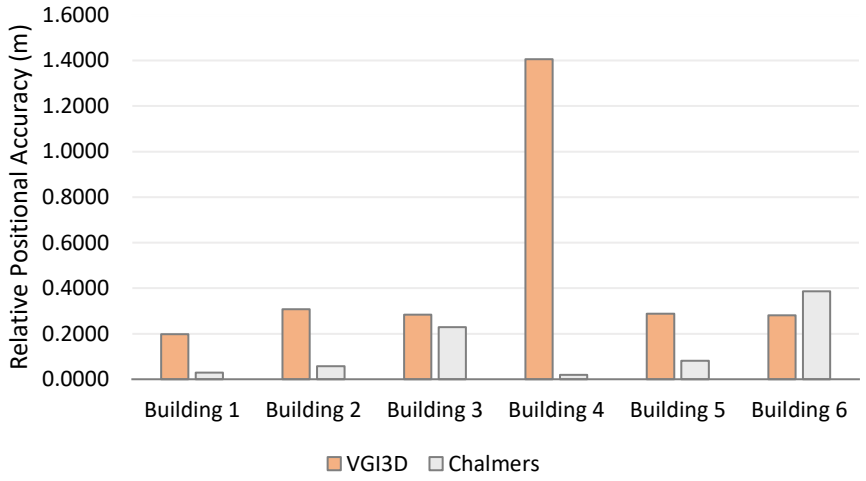

Figure 4.12: The relative positional accuracy of each analyzed building from the VGI3D and Chalmers city models.

4.2 Obstruction angle result comparison

In this section, the obstruction angle results are presented. Discussion regarding the most important results, in combination with illustrations, are given in section 5.2.

Table 4.2 shows the maximum obstruction angles (OA) of each 3D city model for all the window groups. The biggest difference is found between Lund municipality and Chalmers for window group 1 (DSM – 0.5m), where the max Lund municipality OA is 18.50 degrees higher than Chalmers' max OA. The smallest difference is between Lund municipality and Chalmers for window group 2 (DSM – 0.5m), where only 1.24 degrees separate the max OA-values.

Comparing the two DSM resolutions, we generally see small differences. The biggest difference is for Lund municipality group 2, where the 0.5 m DSM is 1.67 degrees higher than the 1 m DSM. The smallest difference is found in window group 3 for the Chalmers model, where the 0.5 m DSM is only 0.01 degrees higher.

Table 4.2: The maximum obstruction angles (degrees) of each 3D city model for all the window groups.

	DSM 1m			DSM 0.5m		
	Lund Mun.	**VGI3D**	**Chalmers**	**Lund Mun.**	**VGI3D**	**Chalmers**
Window group 1	38.42	45.42	21.74	39.88	46.13	21.38
Window group 2	20.80	15.10	23.84	22.47	15.39	23.71
Window group 3	20.46	17.22	11.02	21.66	17.38	11.03

Figure 4.13 is an illustration of the information in Table 4.2.

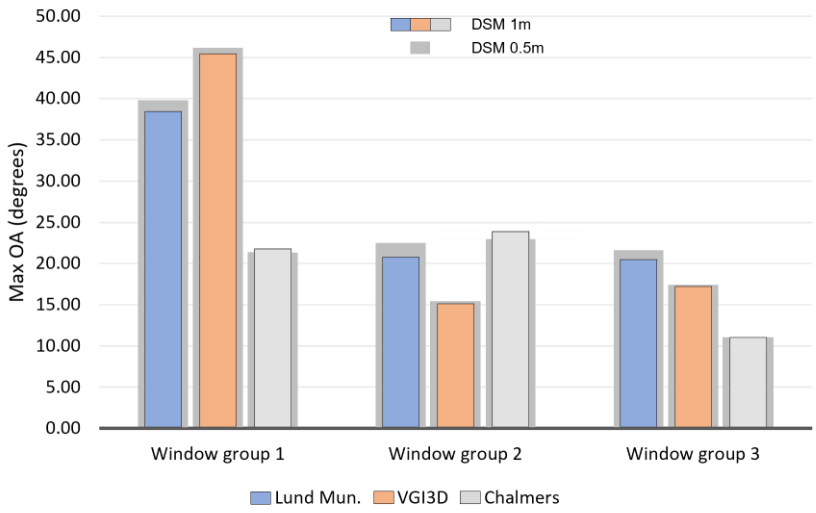

Figure 4.13: The maximum obstruction angles in degrees of each 3D city model for all the window groups. The DSM 1 m values are coloured while corresponding DSM 0.5 m values are underlaid in a grey colour.

Figure 4.14 illustrates the mean difference in OA for all windows in each window group between Lund municipality and VGI3D. For window group 1, VGI3D has, on average, 7.86 degrees higher obstruction angles than Lund municipality. In contrast, for window groups 1 and 2, Lund municipality has the highest obstruction angles, with 2.64 and 2.01 degrees more, respectively.

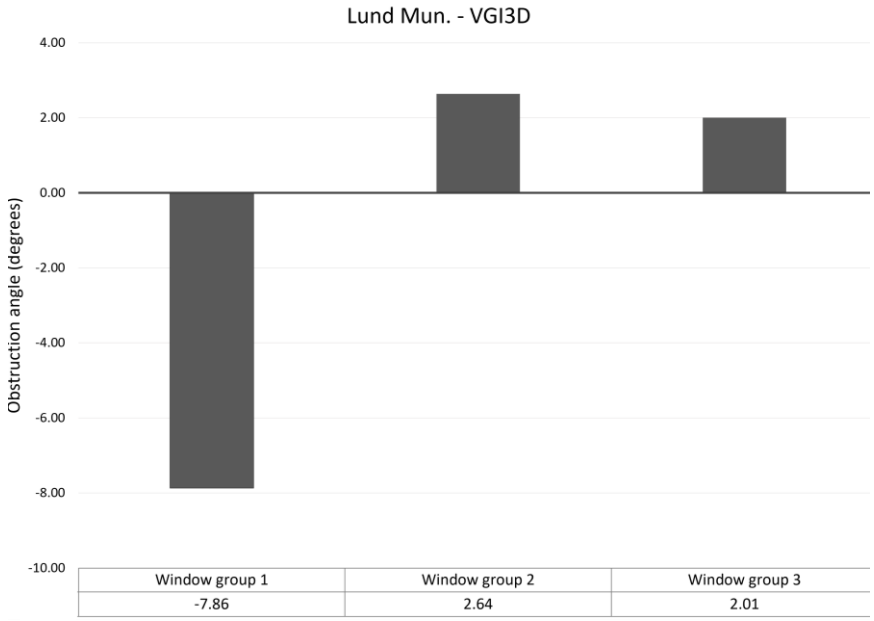

Figure 4.14: The mean difference in obstruction angle degrees for all windows between the Lund municipality and VGI3D models for all three window groups.

Figure 4.15 illustrates the mean difference in obstruction angle for all windows in each window group between Lund municipality and Chalmers. For window group 1, Lund municipality has, on average, 15.02 degrees higher OA than Chalmers. For window group 1, there is only a tiny

difference; Chalmers is 0.97 degrees higher. On average, Lund municipality's windows have 3.99 degrees higher OA's than Chalmers' for window group 3.

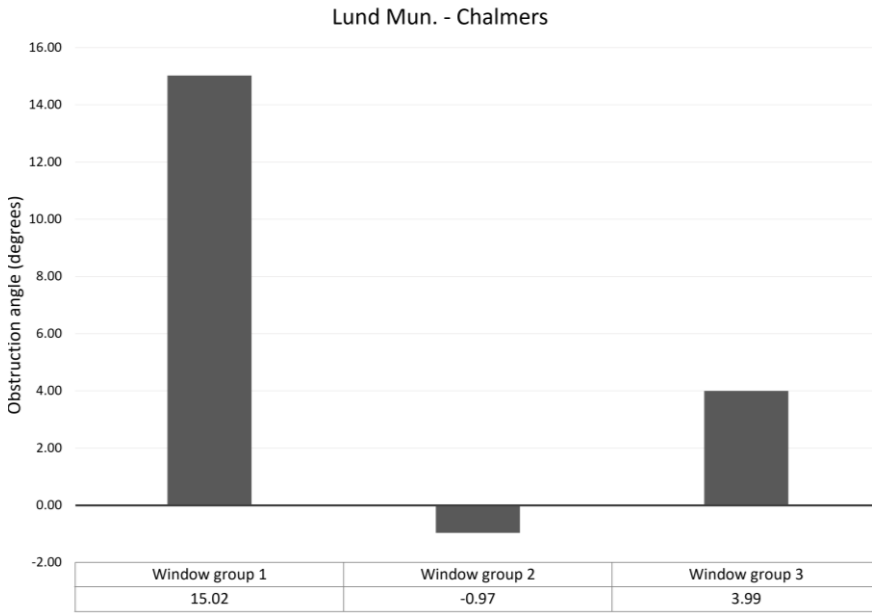

Figure 4.15: The mean difference in obstruction angle degrees for all windows between the Lund municipality and Chalmers models for all three window groups.

5. Discussion

5.1 3D city models

The results chapter shows clear differences between the Lund municipality, VGI3D, and Chalmers 3D city models. Why some of these differences have occurred is discussed in this subchapter. Since the Lund municipality city model is used as the reference model in this thesis, its positional and geometrical accuracy has not been investigated and is therefore not discussed.

VGI3D

The creators of the VGI3D intended to make a platform that could efficiently and conveniently make 3D city models from volunteer geographic information, with window data included. For the city model used in this thesis, a fixed height of 3.8 meters per building storey was used. Their solution is great for efficiency and saving costs, but the downside is that the buildings and objects will often be less true to reality.

An example of when it does not work well is Building 6 (seen in Figure 4.3). As shown in that figure, it is much taller than the Lund municipality building, almost twice as tall at 30 meters, which is much more than reality. Lantmäteriet DSM measures the peak of this building at 14 meters. This difference is likely because the building has unique shapes and window geometry, which is not something the platform is prepared to handle. Figure 5.1 shows what the building looks like in reality. It is a church, and like many churches, it has a very different architecture from most buildings. It is probable that when the VGI3D platform analyzed google street view images of the church, it concluded that there were many more stories than there are.

Figure 5.1: A real picture of Building 6, which has a very inaccurate height in the VGI3D city model. Photo by: Erskine, D. (n.d.).

However, as shown in Figure 4.4, the VGI3D buildings can also be similar in size to Lund municipality buildings. This is assumably the case because the VGI3D platform managed to count the number of floors successfully, and 3.8 meters per storey is a good height for this building. The platform's ability to use different per-storey heights makes it flexible. Therefore, running the platform for a town or city block where you know the height per storey of most buildings will make it much more accurate.

The absolute and positional accuracy of the VGI3D city model gave varying results too. This could be explained by the positional accuracy being based on OSM footprints. A case study by Brovelli, Minghini, Molinari, and Zamboni (2016) found that OSM footprints had a mean difference of about 0.8 m compared to their reference data. These results are similar to this thesis' findings, where, for most buildings, the positional accuracies were under or around half

a meter. Since OSM is a popular data source for generating 3D buildings (e.g., OSM2World and OSM Building), one can assume that VGI3D's positional accuracy could be considered acceptable for simulations. At least where the exact position of the buildings is not of most importance.

For all these reasons, the VGI3D platform is likely more than suitable for many applications that do not require very high positional or geometrical accuracy. Especially if you know the area you will create a city model of beforehand.

Chalmers

The volume and envelope area results of the Chalmers 3D city model were unexpected. Some of the analyzed buildings could be considered accurate, while others were far from it. It is unexpected because the model is made from governmental 3D point data, which one would expect to be accurate. However, without deep knowledge of Chalmers' platform, it is difficult to conclude why two buildings had much less volume and envelope area than Lund's. Personal communication with Dag Wästberg, one of the creators of the Chalmers 3D city model, explained it as uncertain data caused by the data they had received. Many of the buildings have been rebuilt after the governmental 3D point data was last updated, which is seen as the main problem. In one case related to Building 3 (Figure 4.4), The creators of the Chalmers data claim that there were trees in that area instead of the current building when the point data was taken. The algorithm then interprets these trees as a building and gets "confused". This also applies to Building 1. The creators did not check the other buildings analyzed in this thesis; therefore, it is unknown if the same uncertainties apply to them. Likely, the four buildings (2, 4, 5, and 6) have no issues with their data. However, even though these four buildings gave good results, it cannot be determined if this was only a coincidence without further investigation.

The absolute and relative positional accuracy was very good for Chalmers' buildings compared to VGI3D's. For every building, except Building 6, Chalmers has a lower RMSE. Chalmers' absolute and relative positional accuracy RMSE is low even for the two buildings confirmed bugged. This could be explained by their tool using a set of 2D building footprints (Lantmätriet Fastighetskartan) to place the buildings. These footprints must be unaffected by the uncertainties in the 3D point data.

To conclude, judging the Chalmers city model based on the data used in this thesis is unfair, as they deemed some of it as uncertain. Yet, those buildings not confirmed uncertain gave satisfactory results. Further investigation and testing of their city models would be required to come to any real conclusions about the accuracy of their modelling approach.

5.2 The obstruction angle tool

To the author's knowledge, before this thesis, there did not exist a tool that could automatically calculate the obstruction angle of 3D city windows in a GIS environment. To the author's understanding, the most common way of calculating obstruction angles is by doing it manually. Either by inserting the height of the window, obstruction object, and the distance between them into the relevant mathematical formula or by printing a 2D section to measure the angles by hand. These steps must then be done for every window you want to find the obstruction angle.

In contrast, you can click on a single button and wait for it to output all the results through the tool developed in this thesis. Therefore, this tool can hopefully be helpful for many ArcGIS Pro users working with daylight access.

Nevertheless, the tool has some limitations that will be discussed next.

5.2.1 Limitations

The limitations of the obstruction angle tool can be classified into four main categories:

- Limitations due to general inconsistencies in or lack of input data
- Limitations of what type of windows can be analyzed
- Limitations of efficiency due to time-consuming processes
- Limitations of the obstruction angle search direction

The first category refers to general errors in 3D city models and the lack of available window data for these models. This applies to both the creation of 3D city models and the use of the obstruction angle tool. Most 3D city models that are publicly available are from governmental organizations, and these models rarely have higher LoD than 2, meaning they do not include window data (Gröger & Plümer, 2012). And neither is it common for 3D window information to be available separately. Furthermore, inconsistencies in 3D city models have to be assumed, and as this thesis shows, it varies greatly depending on how the models are made. F. Biljecki et al. (2016) state that CityGML datasets are rarely without errors, e.g., missing or not connected pieces and "floating" buildings. They continue by saying that if the models are without errors, they are most likely simple LoD1 models. Therefore, the limitations mentioned in this category affect the obstruction angle tool by making it less accurate due to general errors in 3D city models and less accessible for many because of the lack of available window data.

The second category concerns the type of windows that can be analyzed, which affects an essential part of the tool: finding what direction is perpendicular to the window, as only obstructions in this direction are considered. This tool draws a straight line across the analyzed window (seen in 2D). It then calculates this line's direction (e.g., north to south). The opposite direction of this will then be the perpendicular viewing direction of the window (east to west) (illustrated in Figure 3.7). Since the tool uses a viewshed tool, only one of the directions will be considered, as the building will block the other direction. Hence, if you view the window in 2D and it is not a straight line (the window is not vertical), the tool developed in this thesis will not work correctly. It will still work, but it will act as if the window is vertical, meaning the location of the window midpoint will likely be incorrect. Non-rectangle shaped windows will also have issues with the viewing direction. This limitation is important for users who know they will include such windows in their simulations.

The third category refers to the efficiency of the tool. The obstruction angle tool combines 45 different ArcGIS Pro tools with additional python code. Some of these tools are heavy processes, such as calculating values or angles for hundreds or thousands of raster cells. As a result, the tool is relatively slow. The tool uses about 2 minutes on average per window from my tests (1 and 0.5 m resolution DSMs). One of the window groups consisting of 28 windows will require approximately an hour to run. High-resolution DSMs also take longer to compute

compared to low resolution. At least from my tests, the 0.5-meter DSM took longer than the 1-meter resolution most of the time. However, there were considerable variations in the run-times from the different window groups and resolutions, sometimes, it took 2 hours, and other times it took 30 minutes. Therefore, more testing would be required to determine how big the difference between the two DSM resolutions is. Additionally, it is important to keep in mind that the tool's runtime depends on the user's hardware. All things considered, I am sure there are many ways of improving the tool's efficiency that I have not found or had time to test. Especially if you were to build the tool from scratch without relying on existing ArcGIS Pro tools, there would be many possibilities.

The fourth and final limitation is about the search direction of the tool. A limitation of the obstruction angle metric is that it only looks for obstructions perpendicularly. This limitation could also be applied to the tool created in this thesis, and it has a simple solution: increase the search direction from the window to something broader than perpendicular. However, this would raise new questions, should you look for all obstructions outside the window, even those 90 degrees to the side, although these would block much less daylight on average than something right in front of the window? For this reason, to keep it consistent and straightforward, only obstructions perpendicular to the window was included in this thesis. As a future improvement of the tool, it would be possible to have an option in the GUI for the user to choose how many degrees the search direction should be.

5.2.2 Comparison results

When comparing the OA differences of all windows in window group 1 for the Lund municipality and VGI3D city models (illustrated in Figure 5.2), the VGI3D values are always higher. In this figure, negative values are how many more degrees higher the VGI3D windows are than Lund's. The results for this example are understandable, the opposite VGI3D building is taller, so the OA-values are higher for this model. Yet, the distribution of where the differences are the largest is interesting. The difference increases as the windows get higher, except for the top floor, where the difference is smaller again. This is because the 2.1 meters difference in the height of the opposing buildings has the least impact on the bottom floor. In other words, the height difference from the bottom window to the top of the opposite Lund municipality building is 18.4 meters (20.9 - 2.5), while for the second-highest window, it is 4.9 meters (20.9 - 16). Hence, increasing the height by 2.1 meters will have a more significant effect on the second-highest window than the bottom one. The top row of windows is the exception to this rule because they are so tall that they can see one of the buildings behind the closest building (not in view in Figure 5.2) in the Lund municipality model. Therefore, in their case, it is not a 2.1 meters difference between the two city models but rather a completely different calculation regarding height and distance between the windows and obstructions. There are also some variations in the OA-value-differences at the same window rows. This is because of the different distances from the windows to the obstructions since the two facades facing each other are neither completely straight nor parallel.

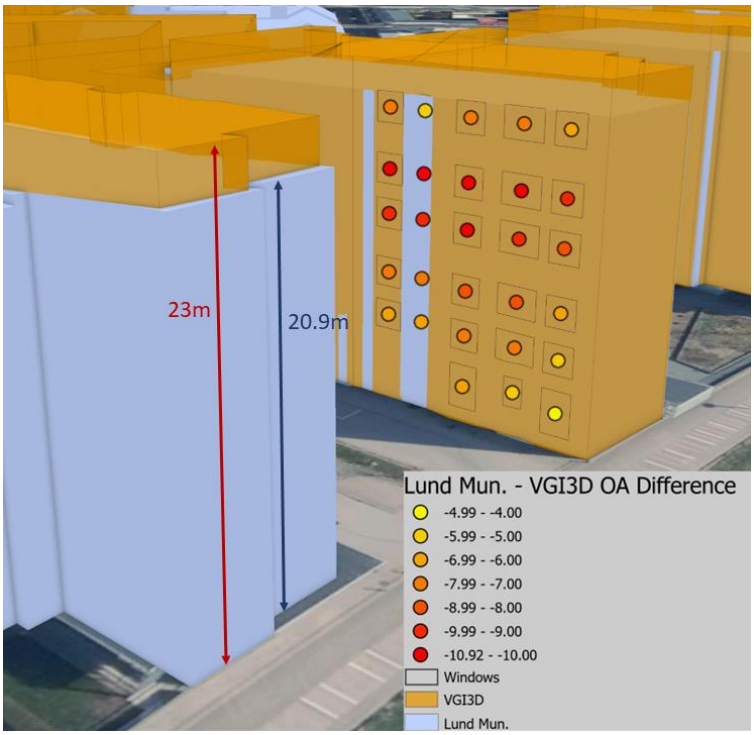

Figure 5.2: The Lund municipality and VGI3D city models overlaid with the difference of the obstruction angle values for window group 1 illustrated (DSM 0.5 m). Each point is the midpoint of a window. Negative values mean how many more degrees the obstruction angle is for the VGI3D windows.

Looking at window group 1 again, this time for Lund municipality and Chalmers, we see quite different results than Figure 5.2. As Figure 5.3 shows, the Chalmers building with the windows is so short that the windows reach higher than the facade. As a result, there was trouble using a viewshed analysis for this window group. Correspondingly, this is one of the issues with using the same window data for different models. The opposing building to the window group is also clearly much shorter than Lund's (due to uncertain data – explained in section 5.1). Therefore, the obstruction angle values are lower for Chalmers in this case. In this example, the Lund municipality windows have greater OA-values for all windows.

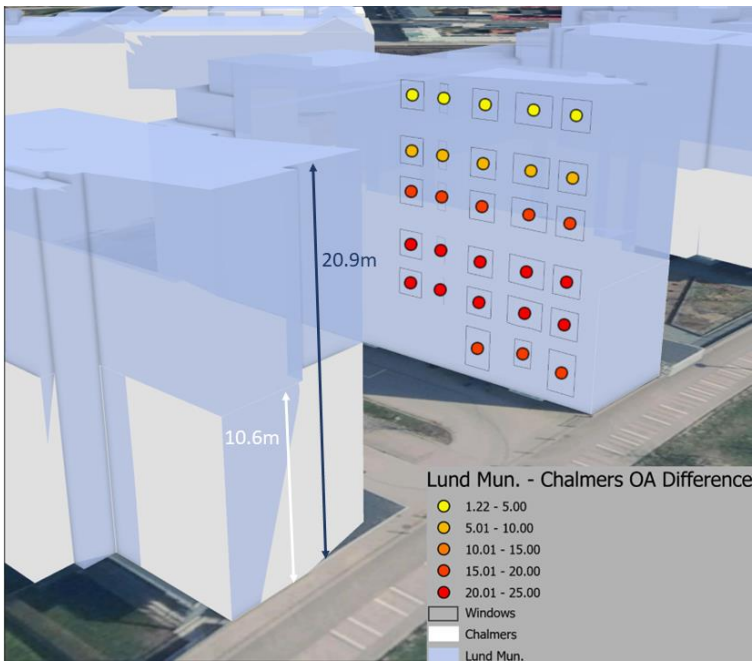

Figure 5.3: The Lund municipality and Chalmers city models overlaid with the difference of the obstruction angle values for window group 1 illustrated (DSM 0.5 m). Each point is the midpoint of a window. Positive values mean how many more degrees the obstruction angle is for the Lund municipality windows than Chalmers.

The difference in mean obstruction angle for window group 2 between Lund municipality and Chalmers is the smallest out of any window group (as shown in Figure 4.14). Figure 5.4

illustrates this difference. The differences are slightly less than zero for almost all windows, meaning the Chalmers model has marginally higher values. This makes sense based on the illustration because the opposing Chalmers' buildings (white) cover more area.

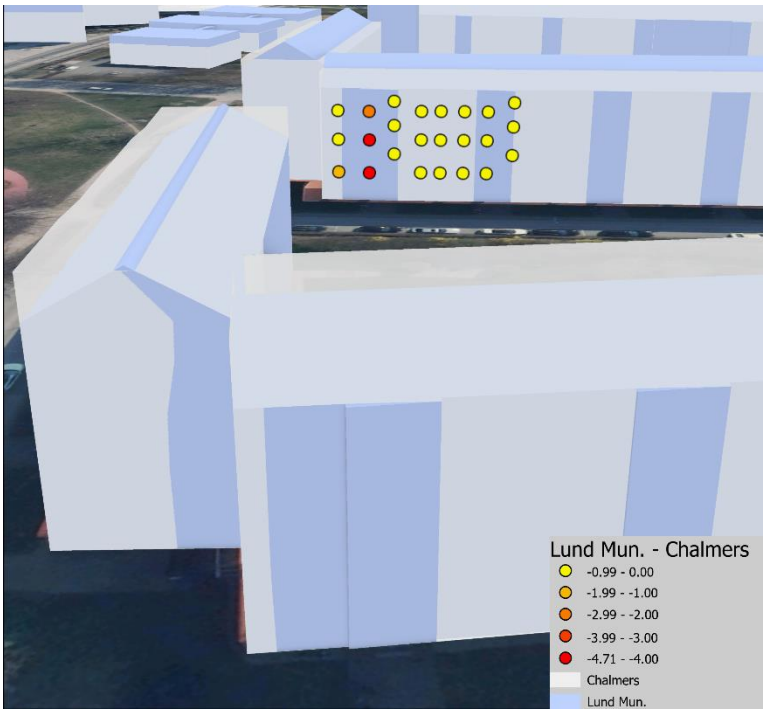

Figure 5.4: The Lund municipality and Chalmers city models overlayed with the difference of the obstruction angle values for window group 2 illustrated (DSM 0.5 m). Each point is the midpoint of a window. Negative values mean how many more degrees the obstruction angle is for the Chalmers windows compared to Lund municipality.

Figure 5.5 shows the difference in obstruction angle values for Lund municipality and VGI3D for window group 3. This is the window group with the smallest difference in mean OA between Lund and VGI3D and the second smallest overall. The figure shows that most of the opposing buildings are taller in Lund's model. And for this reason, most of the windows have higher OA-values in this model.

There are a few cases in Figure 5.5 where some windows have slightly higher values in the VGI3D model. It is unclear in this illustration, but those windows look in a direction with a tall VGI3D building in the background (outside of the image). This tall building does not exist in Lund's model, most likely because it did not exist when the data was created. The location chosen for the window groups was based on the surrounding environment consisting of the same buildings in each model. The author did not consider this tall building in the background. Buildings that only exist in one or two of the city models should have been removed before running the obstruction angle tool to compare the models more fairly.

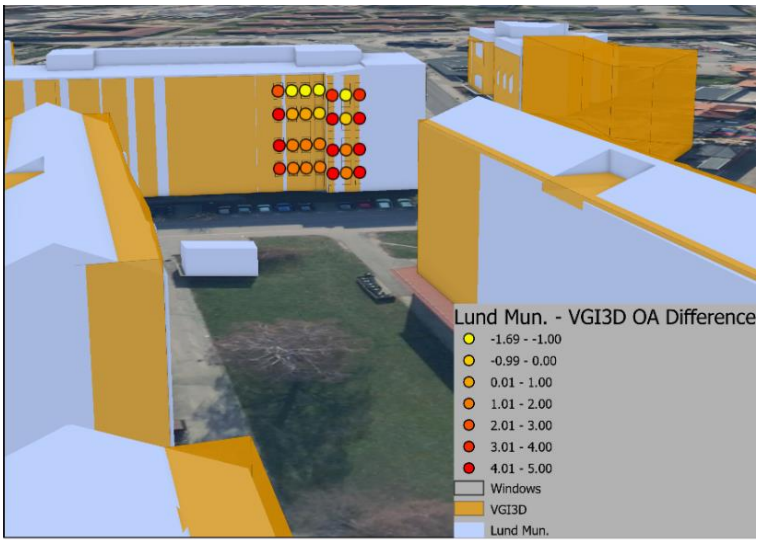

Figure 5.5: The Lund municipality and VGI3D city models overlayed with the difference of the obstruction angle values for window group 3 illustrated (DSM 0.5 m). Each point is the midpoint of a window. Negative values mean how many more degrees the obstruction angle is for the VGI3D windows compared to Lund, and vice versa for positive values.

5.2.3 Significance of the DSM resolution

Table 4.2 shows that there are only minor differences when running the obstruction angle tool with either a 1 m or 0.5 m DSM. This is not surprising since the buildings and windows will still have the same heights at either resolution, meaning the same height values will be used in the calculations. However, the distance from the windows to an obstruction will change slightly. At a higher resolution, more raster cells are registered as obstructions. Therefore, the distance to the closest perpendicular obstruction point will be more precise. Generally, increasing the resolution seems to reduce the distance, making the obstruction angle a little higher (as shown in Figure 4.13). By creating one more DSM for only the area around window group 1 in the VGI3D model, this could be investigated further. The results are seen in Table 5.1. In this case, increasing the resolution to 0.1 meters reduces the distance from the window to the obstructions, which leads to increased obstruction angle values.

Table 5.1: The difference in mean and max OA and distance for window group 1 in the VGI3D model

	Mean OA	Max OA	Mean Distance	Max Distance
DSM 1m	26.81	45.42	21.21	23.39
DSM 0.5m	27.69	46.14	20.33	21.24
DSM 0.1m	28.19	46.54	19.86	20.20

In conclusion, higher DSM resolution is likely to give slightly more accurate results. Still, it is not necessarily significant enough to warrant the increased computational time; this is something the users must take into consideration.

5.3 3D city models and daylight simulations as part of sustainable urban development

As part of the broader term *geodata*, 3D city models and daylight simulations are being used at various levels, both nationally and internationally. 3D city models and other geodata are integral to achieving the United Nations sustainable development goals[19]. Decisions on geodata have

[19] https://sustainabledevelopment.un.org/topics/informationforintegrateddecision-making/geospatialinformation

been made at the national and European Union levels (European Commission, 2021) and the UN level (UN-GGIM 2018, n.d.). A structure for developing federal geodata inside a country was established at the UN. In the EU, the focus is on a standard framework of spatial data between European countries. Regulations and requirements of geodata at both national and international levels must be used as a foundation for developing 3D city models. The existence of a national standard for 3D city models makes inter-municipal collaborations easier, especially for projects close to borders. This is because each municipality is responsible for managing its 3D city model, but they also have access to other 3D city models.

In the study by Kanters et al. (2021), several urban planners stated they do not always have access to or competence in the daylight simulation tools they require. Necessitating the need for an external professional to carry out the simulation, which adds extra costs and extends the time to acquire results. Thus, likely leading to fewer simulations being performed, which further leads to lower quality of sustainable urban development. More simulation tools for 3D city models with small learning curves that are user-friendly are needed. For this reason, the obstruction angle tool developed in this thesis can be helpful.

6. Conclusion

The first research question of this master thesis was to develop an easy-to-use workflow to calculate obstruction angles in a GIS environment. The workflow was intended to help planners, architects, landscape architects, and daylight experts use 3D city solar energy and daylight access simulation tools. The obstruction angle tool created in this thesis is a straightforward tool that only requires two input datasets and no further knowledge of either daylight metrics or 3D city models. Because it does not require any knowledge of the building's interior, it works well with simple 3D city models to provide an indication of daylight access at the early or preliminary stages of the urban planning process. Additionally, it is adapted for an already popular application in the planning process today (ArcGIS Pro). The tool is limited by: the difficulty and cost of obtaining high-quality 3D city models, only being reliable for vertical windows, efficiency due to time-consuming processes, and only being able to search for obstructions in a perpendicular direction.

Albeit the limitations, the obstruction angle tool works as it is supposed to and achieves the first research question. The tool can be improved, especially when it comes to time consumption. Since it is an open-source tool available on GitHub, it can benefit from contributions from other users.

The other research question was to determine how positional accuracy, geometry, LoD, and spatial resolution of 3D building data affect the results of the obstruction angle simulations. From this thesis' results, it is difficult to state precisely how much positional accuracy influenced the windows' obstruction angles because it was not analyzed in isolation. However, there is no question the position of buildings affects obstruction angles, either by changing what is within the search direction or the distance from the window to the obstruction. Geometry had a big effect on the obstruction angles because of the considerable variations in the heights of some buildings. LoD has a high correlation with geometry and similarly affected the obstruction angles mainly due to height differences caused by the detail in roof structures. The spatial resolution of the DSMs used to run the obstruction angle tool had little influence on the obstruction angles. However, this could be caused by the two DSM resolutions tested having relatively high and similar resolution values (1 m and 0.5 m). A much lower resolution would be expected to impact the accuracy of the obstruction angles significantly.

References

Agius, T., Sabri, S., & Kalantari, M. (2018). Three-Dimensional Rule-Based City Modelling to Support Urban Redevelopment Process. *ISPRS International Journal of Geo-Information, 7*(10), 413. Retrieved from https://www.mdpi.com/2220-9964/7/10/413

Ahmed, F. C., & Sekar, S. P. (2015). Using Three-Dimensional Volumetric Analysis in Everyday Urban Planning Processes. *Applied Spatial Analysis and Policy, 8*(4), 393-408. doi:10.1007/s12061-014-9122-2

Alenius, M., Dahlberg, J., Lundgren, M., & Cederström, C. (2019). Dagsljus i Stadsplanering. Retrieved from https://whitearkitekter.com/se/wp-content/uploads/sites/3/2019/04/20190408_WRL_Dagsljus-i-Stadsplanering-1.pdf

Baggerly, C. A., Cuomo, R. E., French, C. B., Garland, C. F., Gorham, E. D., Grant, W. B., . . . Wunsch, A. (2015). Sunlight and Vitamin D: Necessary for Public Health. *Journal of the American College of Nutrition, 34*(4), 359-365. doi:10.1080/07315724.2015.1039866

Basiago, A. D. (1998). Economic, social, and environmental sustainability in development theory and urban planning practice. *Environmentalist, 19*(2), 145-161. doi:10.1023/A:1006697118620

Biljecki, F., Heuvelink, G. B. M., Ledoux, H., & Stoter, J. (2018). The effect of acquisition error and level of detail on the accuracy of spatial analyses. *Cartography and Geographic Information Science, 45*(2), 156-176. doi:10.1080/15230406.2017.1279986

Biljecki, F., Ledoux, H., Du, X., Stoter, J., Soon, K. H., & Khoo, V. H. S. (2016). THE MOST COMMON GEOMETRIC AND SEMANTIC ERRORS IN CITYGML DATASETS. *ISPRS Ann. Photogramm. Remote Sens. Spatial Inf. Sci., IV-2/W1*, 13-22. doi:10.5194/isprs-annals-IV-2-W1-13-2016

Biljecki, F., Ledoux, H., & Stoter, J. (2016). An improved LOD specification for 3D building models. *Computers, Environment and Urban Systems, 59*, 25-37. doi:https://doi.org/10.1016/j.compenvurbsys.2016.04.005

Biljecki, F., Ohori, K., Ledoux, H., Peters, R., & Stoter, J. (2016). Population Estimation Using a 3D City Model: A Multi-Scale Country-Wide Study in the Netherlands. *PloS one, 11*, e0156808. doi:10.1371/journal.pone.0156808

Billen, R., Cutting-Decelle, A.-F., Marina, O., de Almeida, J.-P., M., C., Falquet, G., . . . Zlatanova, S. (2014). 3D City Models and urban information: Current issues and perspectives. *Usage, Usability, and Utility of 3D City Models*, I-118. Retrieved from https://doi.org/10.1051/TU0801/201400001

Bournas, I. (2020). Daylight compliance of residential spaces: Comparison of different performance criteria and association with room geometry and urban density. *Building and Environment, 185*, 107276. doi:https://doi.org/10.1016/j.buildenv.2020.107276

Bournas, I. (2021). Swedish daylight regulation throughout the 20th century and considerations regarding current assessment methods for residential spaces. *Building and Environment, 191*, 107594. doi:10.1016/j.buildenv.2021.107594

Bournas, I., & Dubois, M.-C. (2019). Daylight regulation compliance of existing multi-family apartment blocks in Sweden. *Building and Environment, 150*, 254-265. doi:https://doi.org/10.1016/j.buildenv.2019.01.013

Brovelli, M., Minghini, M., Molinari, M., & Zamboni, G. (2016). POSITIONAL ACCURACY ASSESSMENT OF THE OPENSTREETMAP BUILDINGS LAYER THROUGH AUTOMATIC HOMOLOGOUS PAIRS DETECTION: THE METHOD AND A CASE STUDY. *ISPRS - International Archives of the Photogrammetry, Remote Sensing and Spatial Information Sciences, XLI-B2*, 615-620. doi:10.5194/isprsarchives-XLI-B2-615-2016

buildingSMART. (2022). Industry Foundation Classes (IFC). Retrieved from https://www.buildingsmart.org/standards/bsi-standards/industry-foundation-classes/

Carvalho, J. P., Alecrim, I., Bragança, L., & Mateus, R. (2020). Integrating BIM-Based LCA and Building Sustainability Assessment. *Sustainability, 12*(18), 7468. Retrieved from https://www.mdpi.com/2071-1050/12/18/7468

CIE. (2003). CIE Standard Overcast Sky and Clear Sky. Retrieved from https://cie.co.at/publications/cie-standard-overcast-sky-and-clear-sky

Cillari, G., Fantozzi, F., & Franco, A. (2021). Passive Solar Solutions for Buildings: Criteria and Guidelines for a Synergistic Design. *Applied Sciences, 11*(1), 376. Retrieved from https://www.mdpi.com/2076-3417/11/1/376

CityJSON. (n.d.). CityJSON. Retrieved March 2, 2022. Retrieved from https://www.cityjson.org/

Daly, H. E. (1974). The Economics of the Steady State. *The American Economic Review, 64*(2), 15-21. Retrieved from http://www.jstor.org/stable/1816010

Daneshvar Tarigh, A., Daneshvar Tarigh, F., & Nikranjbar, A. (2012). *A Survey of Energy-Efficient Passive Solar Houses*.

Desthieux, G., Carneiro, C., Camponovo, R., Ineichen, P., Morello, E., Boulmier, A., . . . Ellert, C. (2018). Solar Energy Potential Assessment on Rooftops and Facades in Large Built Environments Based on LiDAR Data, Image Processing, and Cloud Computing. Methodological Background, Application, and Validation in Geneva (Solar Cadaster). *Frontiers in Built Environment, 4*. doi:10.3389/fbuil.2018.00014

Dogan, T., & Knutins, M. (2018). *CitySeek: Towards Urban Daylight Models Based on GIS Data and Semi-Automated Image Processing*.

DTCC. (n.d.). Retrieved February 12, 2022. Retrieved from https://dtcc.chalmers.se/

Duffie, J. A., & Beckman, W. A. (2013). Solar Radiation. In *Solar Engineering of Thermal Processes* (pp. 3-42).

Döllner, J., Baumann, K., & Buchholz, H. (2007). *Virtual 3D City Models as Foundation of Complex Urban Information Spaces*.

Eicker, U., Nouvel, R., Duminil, E., & Coors, V. (2014). Assessing Passive and Active Solar Energy Resources in Cities Using 3D City Models. *Energy Procedia, 57*, 896-905. doi:https://doi.org/10.1016/j.egypro.2014.10.299

Energy, U. S. D. o. (n.d.). Solar Radiation Basics. Retrieved February 17, 2022. Retrieved from https://www.energy.gov/eere/solar/solar-radiation-basics

Environment, S. B. (n.d.). 3CIM – Smarta 3D-stadsmodeller. Retrieved February 2, 2022. Retrieved from https://www.smartbuilt.se/

Eriksson, H., Johansson, T., Olsson, P.-O., Andersson, M., Engvall, J., Hast, I., & Harrie, L. (2020). Requirements, Development, and Evaluation of A National Building Standard—A Swedish Case Study. *ISPRS International Journal of Geo-Information, 9*(2), 78. Retrieved from https://www.mdpi.com/2220-9964/9/2/78

Eriksson, S., & Waldenström, L. (2016). *Daylight in Existing Buildings.* Chalmers University of Technology, Retrieved from https://publications.lib.chalmers.se/records/fulltext/245180/245180.pdf

Erskine, D. (n.d.). Klosterkyrkan. Retrieved from https://www.svenskakyrkan.se/lund/sanktpeterskloster/klosterkyrkan

European-Commission. (2019). From nearly-zero energy buildings to net-zero energy districts. Retrieved from https://ec.europa.eu/jrc/en/news/nearly-zero-energy-buildings-net-zero-energy-districts

European-Commission. (2020). In Focus: Energy efficiency in buildings. Retrieved from https://ec.europa.eu/info/news/focus-energy-efficiency-buildings-2020-feb-17_en

European-Commission. (2021). About INSPIRE. Retrieved from https://inspire.ec.europa.eu/about-inspire/563

European-Commission. (n.d.). Causes of climate change. Retrieved February 17, 2022. Retrieved from https://ec.europa.eu/clima/climate-change/causes-climate-change_en

European-Commission. (n.d.). Energy and the Green Deal. Retrieved February 17, 2022. Retrieved from https://ec.europa.eu/info/strategy/priorities-2019-2024/european-green-deal/energy-and-green-deal_en

European-Commission. (n.d.). Energy performance of buildings directive. Retrieved February 6, 2022. Retrieved from https://energy.ec.europa.eu/topics/energy-efficiency/energy-efficient-buildings/energy-performance-buildings-directive_en

Fan, H., Kong, G., & Zhang, C. (2021). An Interactive platform for low-cost 3D building modeling from VGI data using convolutional neural network. *Big Earth Data, 5*(1), 49-65. doi:10.1080/20964471.2021.1886391

Fan, H., Zipf, A., Fu, Q., & Neis, P. (2014). Quality assessment for building footprints data on OpenStreetMap. *International Journal of Geographical Information Science, 28*, 700-719.

Francisco, A., Mohammadi, N., & Taylor, J. E. (2020). Smart City Digital Twin–Enabled Energy Management: Toward Real-Time Urban Building Energy Benchmarking. *Journal of Management in Engineering, 36*(2), 04019045. doi:doi:10.1061/(ASCE)ME.1943-5479.0000741

Freitas, S., Catita, C., Redweik, P., & Brito, M. C. (2015). Modelling solar potential in the urban environment: State-of-the-art review. *Renewable and Sustainable Energy Reviews, 41*, 915-931. doi:https://doi.org/10.1016/j.rser.2014.08.060

Gilpin, H. (1980). [World Conservation Strategy, International Union for Conservation of Nature and Natural Resources (IUCN)]. *Third World Quarterly, 2*(3), 572-574. Retrieved from http://www.jstor.org/stable/3990937

Gruber, U., Riecken, J., & Seifert, M. (2014). *Germany on the Way to 3 D-Cadastre*.

Gröger, G., Kolbe, T. H., Nagel, C., & Häfele, K.-H. (2012). *OGC City Geography Markup Language (CityGML) Encoding Standard*.

Gröger, G., & Plümer, L. (2012). CityGML – Interoperable semantic 3D city models. *ISPRS Journal of Photogrammetry and Remote Sensing, 71*, 12-33. doi:https://doi.org/10.1016/j.isprsjprs.2012.04.004

Guptill, S. C., & Morrison, J. L. (2013). *Elements of spatial data quality*: Elsevier.

Hamersma, M., Haas, M., & Faber, R. (2020). Thuiswerken en de coronacrisis. *Een overzicht van studies naar de omvang, beleving en toekomstverwachting van thuiswerken in coronatijd. Den Haag, Kennisinstituut voor Mobiliteitsbeleid (KiM)*.

Harrie, L., Kanters, J., Mattisson, K., Nezval, P., Olsson, P. O., Pantazatou, K., . . . Fan, H. (2021). 3D CITY MODELS FOR SUPPORTING SIMULATIONS IN CITY DENSIFICATIONS. *Int. Arch. Photogramm. Remote Sens. Spatial Inf. Sci., XLVI-4/W4-2021*, 73-77. doi:10.5194/isprs-archives-XLVI-4-W4-2021-73-2021

Hemnet. (2020). Efter pandemin – Lämnar vi stan då? . Retrieved from https://www.hemnet.se/artiklar/bostadsmarknaden/2020/10/28/efter-pandemin-lamnar-vi-stan-nu

Huang, W., Olsson, P. O., Kanters, J., & Harrie, L. (2020). RECONCILING CITY MODELS WITH BIM IN KNOWLEDGE GRAPHS: A FEASIBILITY STUDY OF DATA INTEGRATION FOR SOLAR ENERGY SIMULATION. *ISPRS Annals of Photogrammetry, Remote Sensing and Spatial Information Sciences, VI-4/W1-2020*, 93-99. doi:10.5194/isprs-annals-VI-4-W1-2020-93-2020

Huang, X., Huang, J., Wen, D., & Li, J. (2021). An updated MODIS global urban extent product (MGUP) from 2001 to 2018 based on an automated mapping approach. *International Journal of Applied Earth Observation and Geoinformation, 95*, 102255. doi:https://doi.org/10.1016/j.jag.2020.102255

Haaland, C., & van den Bosch, C. K. (2015). Challenges and strategies for urban green-space planning in cities undergoing densification: A review. *Urban Forestry & Urban Greening, 14*(4), 760-771. doi:https://doi.org/10.1016/j.ufug.2015.07.009

ISO. (2003). ISO 19107:2003: Geographic information—Spatial schema. International Organization for Standardization.

Jakica, N. (2017). State-of-the-art review of solar design tools and methods for assessing daylighting and solar potential for building-integrated photovoltaics. *Renewable and Sustainable Energy Reviews, 81*. doi:10.1016/j.rser.2017.05.080

Jamrozik, A., Clements, N., Hasan, S. S., Zhao, J., Zhang, R., Campanella, C., . . . Bauer, B. (2019). Access to daylight and view in an office improves cognitive performance and satisfaction and reduces eyestrain: A controlled crossover study. *Building and Environment, 165*, 106379. doi:https://doi.org/10.1016/j.buildenv.2019.106379

Kanters, J., & Davidsson, H. (2017). Assessing combined object and mutual shading on the performance of a solar field. Retrieved from http://www.buildingsimulation2017.org/

Kanters, J., Gentile, N., & Bernardo, R. (2021). Planning for solar access in Sweden: routines, metrics, and tools. *Urban, Planning and Transport Research, 9*(1), 347-367. doi:10.1080/21650020.2021.1944293

Kanters, J., Wall, M., & Kjellsson, E. (2014). The Solar Map as a Knowledge Base for Solar Energy Use. *Energy Procedia, 48*, 1597-1606. doi:https://doi.org/10.1016/j.egypro.2014.02.180

Knier, G. (2008). How to Photovoltaics work? Retrieved from https://science.nasa.gov/science-news/science-at-nasa/2002/solarcells

Kong, G., & Fan, H. (2021). Enhanced Facade Parsing for Street-Level Images Using Convolutional Neural Networks. *IEEE Transactions on Geoscience and Remote Sensing, 59*(12), 10519-10531. doi:10.1109/TGRS.2020.3035878

Kutzner, T., Chaturvedi, K., & Kolbe, T. H. (2020). CityGML 3.0: New Functions Open Up New Applications. *PFG – Journal of Photogrammetry, Remote Sensing and Geoinformation Science, 88*(1), 43-61. doi:10.1007/s41064-020-00095-z

Lancelle, M., & Fellner, D. W. (2004). Current issues on 3D city models.

Lantmäteriet. (2018). Mätanvisningar Geometrisk representation vid utbyte Version 3.2.

Ledoux, H. (2018). val3dity: validation of 3D GIS primitives according to the international standards. *Open Geospatial Data, Software and Standards, 3*(1), 1. doi:10.1186/s40965-018-0043-x

Ledoux, H., Arroyo Ohori, K., Kumar, K., Dukai, B., Labetski, A., & Vitalis, S. (2019). CityJSON: a compact and easy-to-use encoding of the CityGML data model. *Open Geospatial Data, Software and Standards, 4*(1), 4. doi:10.1186/s40965-019-0064-0

Lee, S. C., & Nevatia, R. (2004). *Extraction and integration of window in a 3D building model from ground view images* (Vol. 2).

Lindberg, F., Grimmond, C. S. B., Gabey, A., Huang, B., Kent, C. W., Sun, T., . . . Zhang, Z. (2018). Urban Multi-scale Environmental Predictor (UMEP): An integrated tool for city-based climate services. *Environmental Modelling & Software, 99*, 70-87. doi:https://doi.org/10.1016/j.envsoft.2017.09.020

Lindberg, F., Jonsson, P., Honjo, T., & Wästberg, D. (2015). Solar energy on building envelopes – 3D modelling in a 2D environment. *Solar Energy, 115*, 369-378. doi:https://doi.org/10.1016/j.solener.2015.03.001

Littlefair, P. (2001). Daylight, sunlight and solar gain in the urban environment. *Solar Energy, 70*(3), 177-185. doi:https://doi.org/10.1016/S0038-092X(00)00099-2

Littlefair, P. (2011). Site layout planning for daylight and sunlight. Retrieved from https://images.reading.gov.uk/2021/07/BRE-Oct-2011-Site-layout-planning-for-Daylight-and-sunlight.pdf

Lorek, S. (2022). What is BIM? . Retrieved from https://constructible.trimble.com/construction-industry/what-is-bim-building-information-modeling

Lwin, K., & Murayama, Y. (2009). A GIS Approach to Estimation of Building Population for Micro-spatial Analysis. *Transactions in GIS, 13*(4), 401-414. doi:https://doi.org/10.1111/j.1467-9671.2009.01171.x

Mardaljevic, J., Heschong, L., & Lee, E. (2009). Daylight metrics and energy savings. *Lighting Research & Technology - LIGHTING RES TECHNOL, 41*, 261-283. doi:10.1177/1477153509339703

Marszal, A. J., Heiselberg, P., Bourrelle, J. S., Musall, E., Voss, K., Sartori, I., & Napolitano, A. (2011). Zero Energy Building – A review of definitions and calculation methodologies. *Energy and Buildings, 43*(4), 971-979. doi:https://doi.org/10.1016/j.enbuild.2010.12.022

Mohammadi, N., & Taylor, J. E. (2017, 27 Nov.-1 Dec. 2017). *Smart city digital twins.* Paper presented at the 2017 IEEE Symposium Series on Computational Intelligence (SSCI).

Nezval, P. (2021). *Design, implementation and evaluation of a daylight estimation tool using 3D city model data.* (Master). Lund University, http://lup.lub.lu.se/student-papers/record/9068031.

Noardo, F., Arroyo Ohori, K., Biljecki, F., Ellul, C., Harrie, L., Krijnen, T., . . . Stoter, J. (2021). Reference study of CityGML software support: The GeoBIM benchmark 2019—Part II. *Transactions in GIS, 25*(2), 842-868. doi:https://doi.org/10.1111/tgis.12710

Nordlander, M. (2020). Vill människor ha andra bostäder efter corona? . Retrieved from https://www.fastighetsnytt.se/fastighetsmarknad/bostader/vill-manniskor-ha-andra-bostader-efter-corona/

Nouvel, R., Mastrucci, A., Leopold, U., Baume, O., Coors, V., & Eicker, U. (2015). Combining GIS-based statistical and engineering urban heat consumption models: Towards a new framework for multi-scale policy support. *Energy and Buildings, 107*, 204-212. doi:https://doi.org/10.1016/j.enbuild.2015.08.021

Næss, P., Saglie, I.-L., & Richardson, T. (2020). Urban sustainability: is densification sufficient? *European Planning Studies, 28*(1), 146-165. doi:10.1080/09654313.2019.1604633

OGC. (2021). OGC Membership approves the CityGML v3.0 Conceptual Model as official OGC Standard [Press release]. Retrieved from https://www.ogc.org/pressroom/pressreleases/4555

OGC. (n.d.-a). CityGML. Retrieved March 3, 2022. Retrieved from https://www.ogc.org/standards/citygml

OGC. (n.d.-b). CityJSON Community Standard 1.0. . Retrieved from https://docs.ogc.org/cs/20-072r2/20-072r2.html'

Peronato, G., Bonjour, S., Stoeckli, J., Rey, E., & Andersen, M. (2016). *Sensitivity of calculated solar irradiation to the level of detail: insights from the simulation of four sample buildings in urban areas*.

Pierce, P., & Andersson, B. (2017). *Challenges with smart cities initiatives – A municipal decision makers' perspective*.

Pradhan, B. (2017). *Spatial Modeling and Assessment of Urban Form Analysis of Urban Growth: From Sprawl to Compact Using Geospatial Data*.

Pyle, R., Bentzien, M., & Opler, P. (1981). Insect Conservation. *Annual Review of Entomology, 26*(1), 233-258. doi:10.1146/annurev.en.26.010181.001313

Saving, C. C. f. R. E. S. a. (n.d.). Active Solar Systems. Retrieved February 18, 2022. Retrieved from http://www.cres.gr/kape/energeia_politis/energeia_politis_active_solar_uk.htm

Schebek, L., Schnitzer, B., Blesinger, D., Köhn, A., Miekley, B., Linke, H. J., . . . Seemann, A. (2017). Material stocks of the non-residential building sector: the case of the Rhine-Main area. *Resources, Conservation and Recycling, 123*, 24-36. doi:https://doi.org/10.1016/j.resconrec.2016.06.001

Schindler, K., & Bauer, J. (2003, 17-17 Oct. 2003). *A model-based method for building reconstruction.* Paper presented at the First IEEE International Workshop on Higher-Level Knowledge in 3D Modeling and Motion Analysis, 2003. HLK 2003.

SHC. (2021). Taking Solar Neighborhood Tools to the Classroom. Retrieved from https://task63.iea-shc.org/Data/Sites/1/publications/2021-12-Task63-Taking-Solar-Neighborhood-Tools-to-the-Classroom.pdf

SIG3D. (2018). Modeling Guide for 3D Objects Part 2: Modeling of Buildings (LoD1, LoD2 and LoD3). Retrieved from https://en.wiki.quality.sig3d.org/index.php?title=Modeling_Guide_for_3D_Objects_-_Part_2:_Modeling_of_Buildings_(LoD1,_LoD2,_LoD3)

Soon, K., & Khoo, V. (2017). CITYGML MODELLING FOR SINGAPORE 3D NATIONAL MAPPING. *ISPRS - International Archives of the Photogrammetry, Remote Sensing and Spatial Information Sciences, XLII-4/W7*, 37-42. doi:10.5194/isprs-archives-XLII-4-W7-37-2017

Stoter, J., Ledoux, H., Reuvers, M., Klooster, L. a. R., Janssen, P., Beetz, J., . . . Vosselman, G. (2013). Establishing and implementing a national 3D standard in The Netherlands: Entwicklung und

Implementierung eines nationalen 3D Standards in den Niederlanden. *Photogrammetrie Fernerkundung Geoinformation, 2013*, 381--392. doi:10.1127/1432-8364/2013/0184

Stoter, J., Vosselman, G., Goos, J., Zlatanova, S., Verbree, E., Klooster, R., & Reuvers, M. (2011). Towards a National 3D Spatial Data Infrastructure: Case of The Netherlands. *Photogrammetrie - Fernerkundung - Geoinformation*, 405-420. doi:10.1127/1432-8364/2011/0094

Strømann-Andersen, J., & Sattrup, P. A. (2011). The urban canyon and building energy use: Urban density versus daylight and passive solar gains. *Energy and Buildings, 43*(8), 2011-2020. doi:https://doi.org/10.1016/j.enbuild.2011.04.007

Swedish-Standard. (1987). Byggnadsutformning - Dagsljus - Förenklad metod för kontroll av erforderlig fönsterglasarea.

Theodoridou, I., Karteris, M., Mallinis, G., Papadopoulos, A., & Hegger, M. (2012). Assessment of retrofitting measures and solar systems' potential in urban areas using Geographical Information Systems: Application to a Mediterranean city. *Renewable and Sustainable Energy Reviews, 16*, 6239–6261. doi:10.1016/j.rser.2012.03.075

Tsalikis, G., & Martinopoulos, G. (2015). Solar energy systems potential for nearly net zero energy residential buildings. *Solar Energy, 115*, 743-756. doi:https://doi.org/10.1016/j.solener.2015.03.037

United-Nations. (2018). 68% of the world population projected to live in urban areas by 2050, says UN. Retrieved from https://www.un.org/development/desa/en/news/population/2018-revision-of-world-urbanization-prospects.html

United-Nations. (2019). Population Divisions. Retrieved from https://population.un.org/wpp/

United-Nations. (2020). Urban Climate Action Is Crucial to Bend the Emission Curve. Retrieved from https://unfccc.int/news/urban-climate-action-is-crucial-to-bend-the-emissions-curve

United-Nations. (n.d.). UN-GGIM. Retrieved January 26, 2022. Retrieved from https://ggim.un.org/unwgic/

van den Brink, L., Stoter, J., & Zlatanova, S. (2013). Establishing a national standard for 3D topographic data compliant to CityGML. *International Journal of Geographical Information Science, 27*(1), 92-113. doi:10.1080/13658816.2012.667105

van der Hoeven, F., & Wandl, A. (2015). Amsterwarm: Mapping the landuse, health and energy-efficiency implications of the Amsterdam urban heat island. *Building Services Engineering Research and Technology, 36*(1), 67-88. doi:10.1177/0143624414541451

van der Rhee, H. J., de Vries, E., & Coebergh, J. W. (2016). Regular sun exposure benefits health. *Medical Hypotheses, 97*, 34-37. doi:https://doi.org/10.1016/j.mehy.2016.10.011

Vitousek, P. M., Mooney, H. A., Lubchenco, J., & Melillo, J. M. (1997). Human Domination of Earth's Ecosystems. *Science, 277*(5325), 494-499. doi:doi:10.1126/science.277.5325.494

Wald, L. (2018). Basics in solar radiation at Earth surface. doi:PDF: https://www.researchgate.net/profile/Lucien-Wald/publication/322314967_BASICS_IN_SOLAR_RADIATION_AT_EARTH_SURFACE/links/5a537a9faca2725638c80224/BASICS-IN-SOLAR-RADIATION-AT-EARTH-SURFACE.pdf

Weller, R. B. (2016). Sunlight Has Cardiovascular Benefits Independently of Vitamin D. *Blood Purification, 41*(1-3), 130-134. doi:10.1159/000441266

Yeh, A. G.-O., & Li, X. (2006). Errors and uncertainties in urban cellular automata. *Computers, Environment and Urban Systems, 30*(1), 10-28. doi:https://doi.org/10.1016/j.compenvurbsys.2004.05.007

Appendix

Appendix A:

Appendix A contains illustrations of all of the six analyzed Chalmers buildings compared to the corresponding Lund municipality buildings.

Building 1:

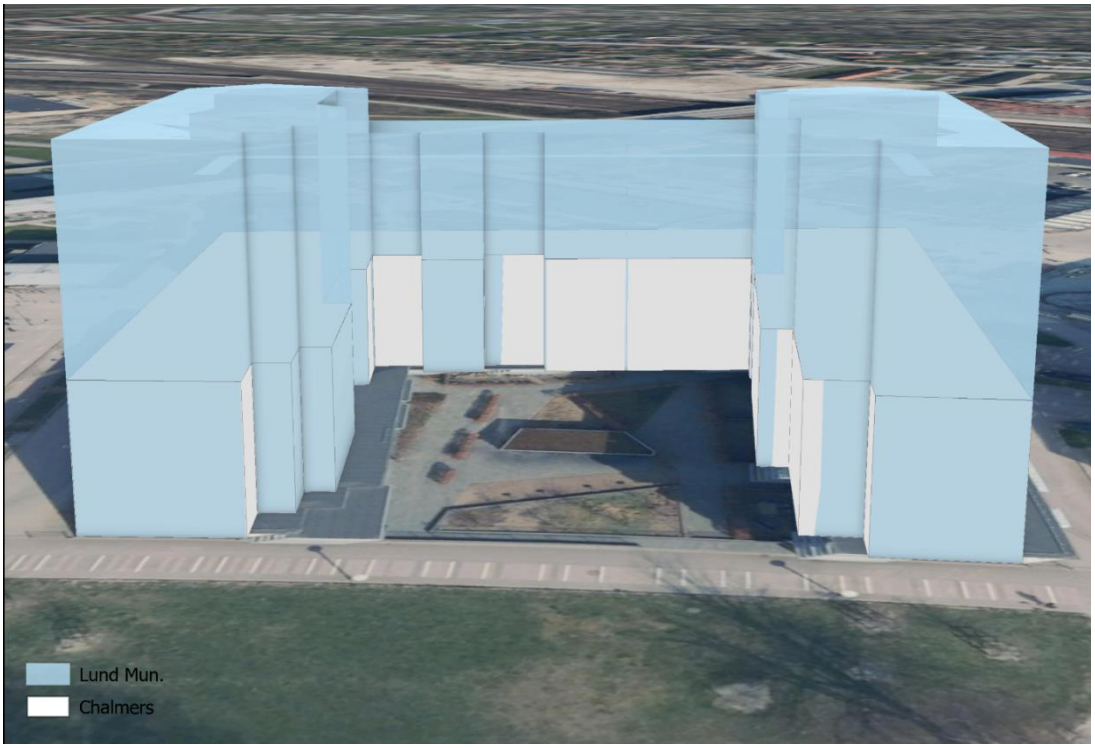

Building 2:

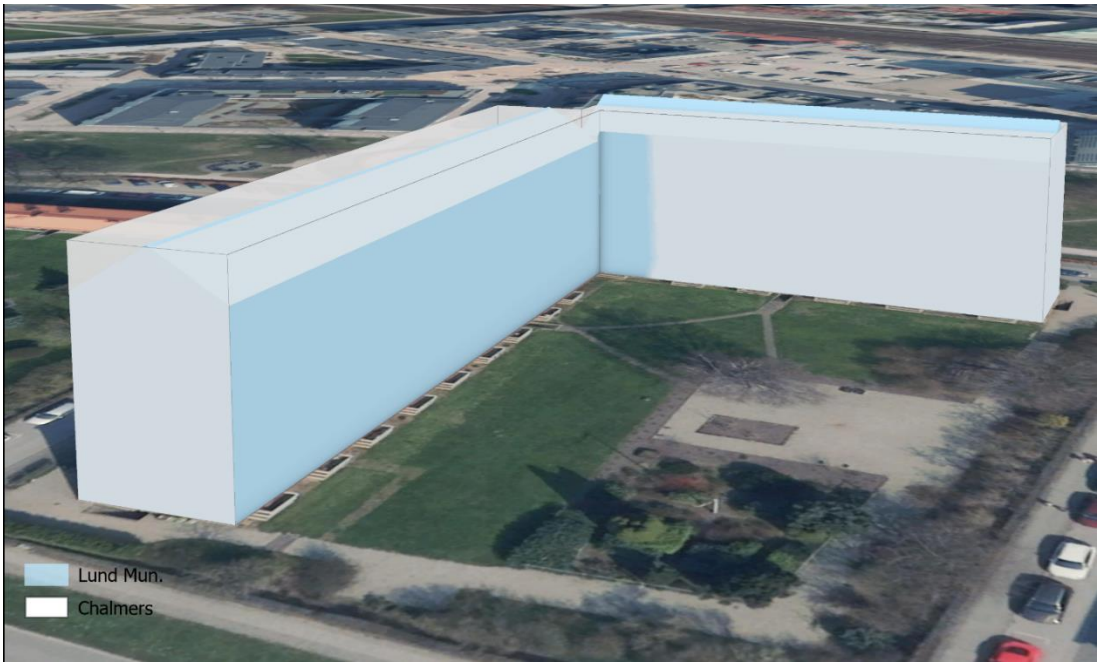

Building 3:

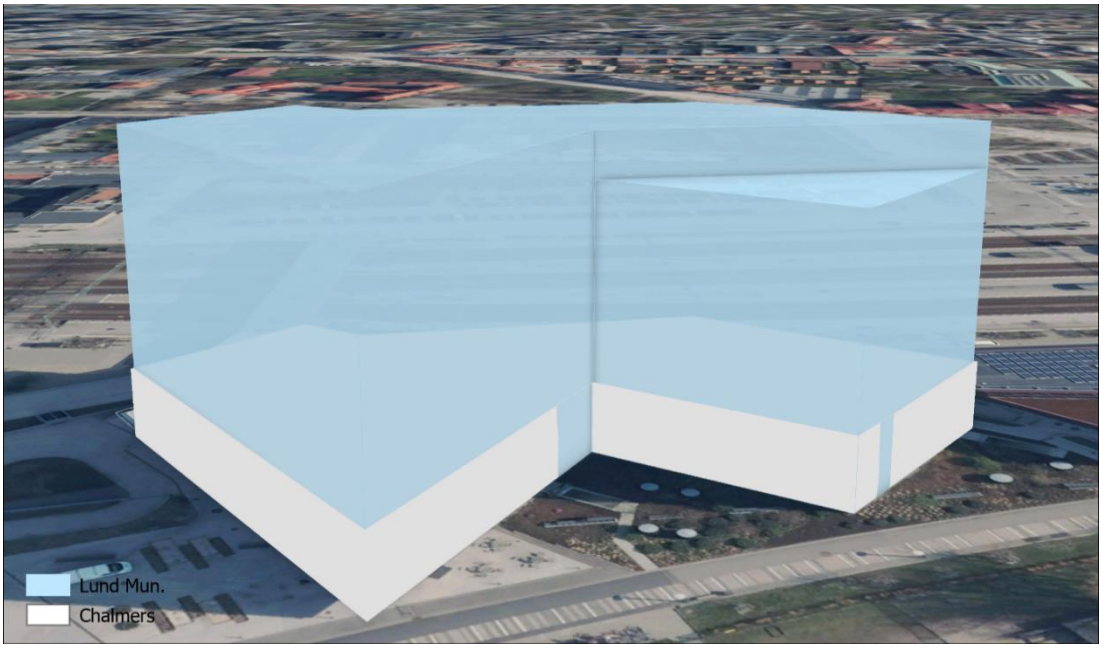

Building 4:

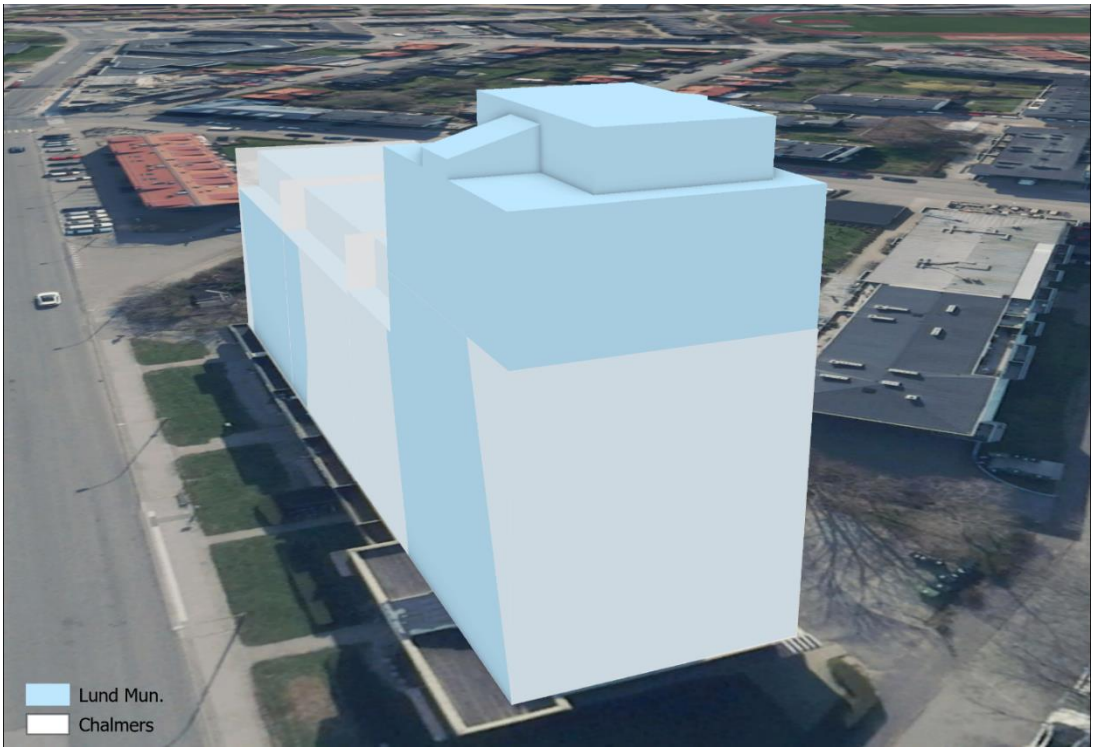

Building 5:

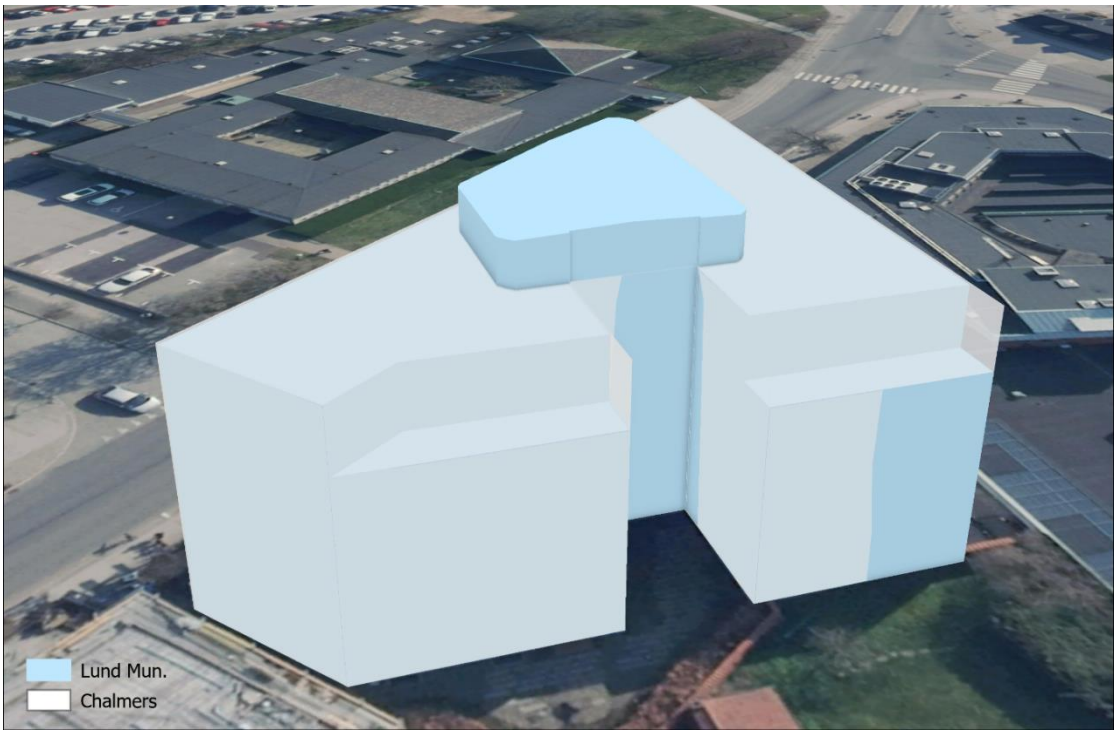

Building 6:

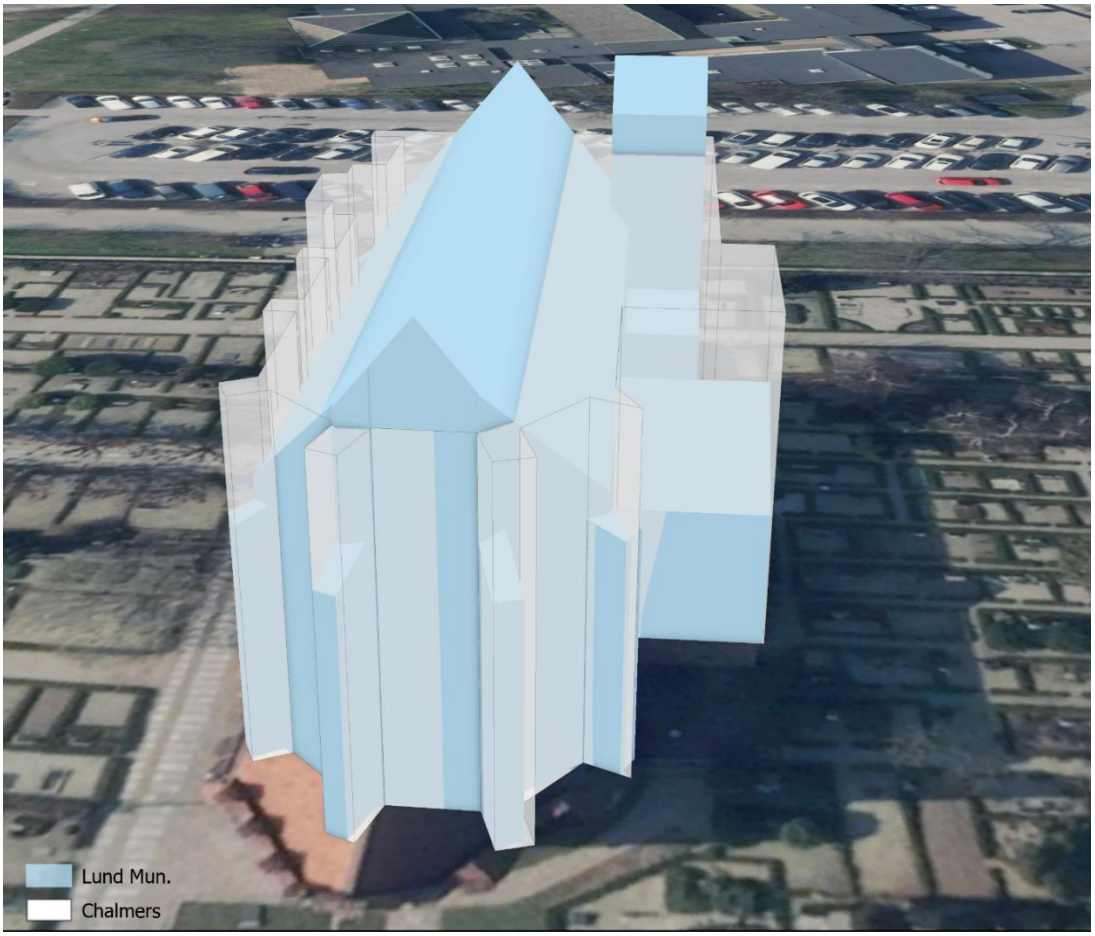

Appendix B:

Appendix B contains illustrations of all of the six analyzed VGI3D buildings compared to the corresponding Lund municipality buildings.

Building 1:

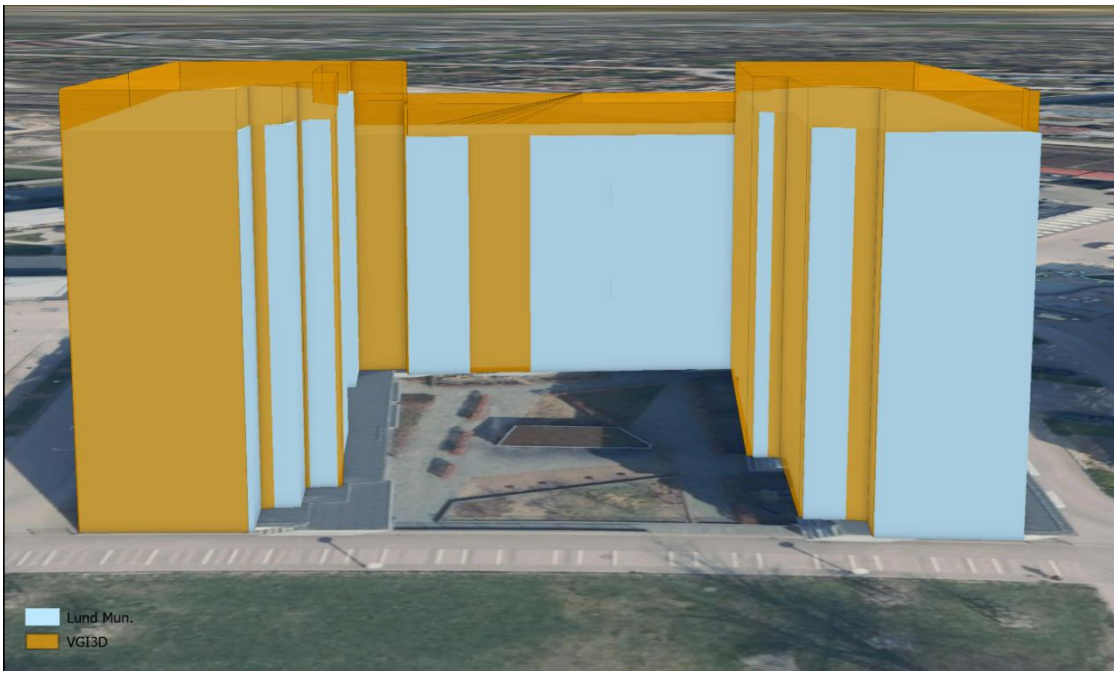

Building 2:

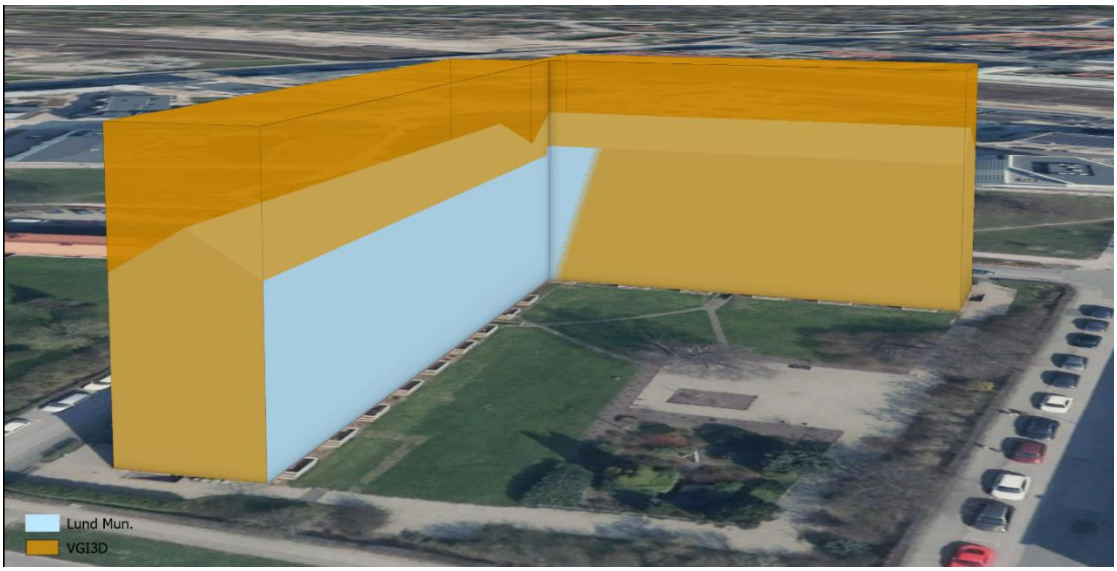

Building 3:

Building 4:

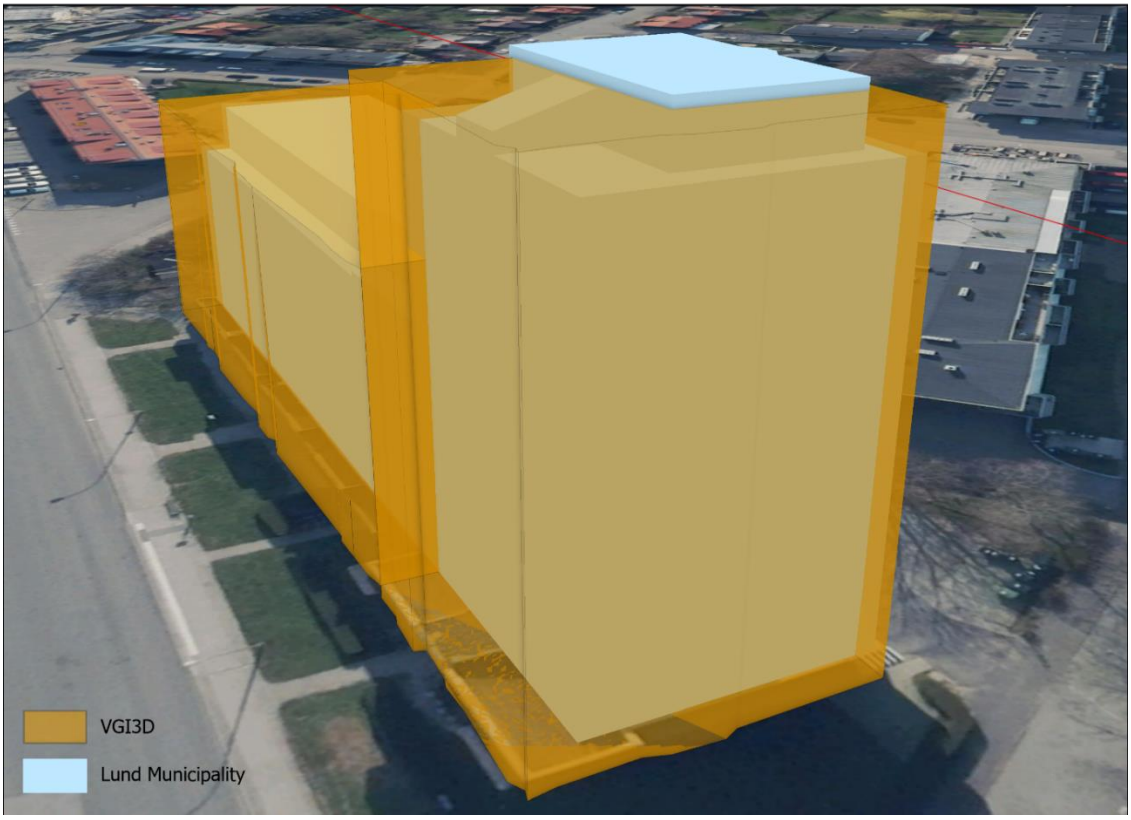

Building 5:

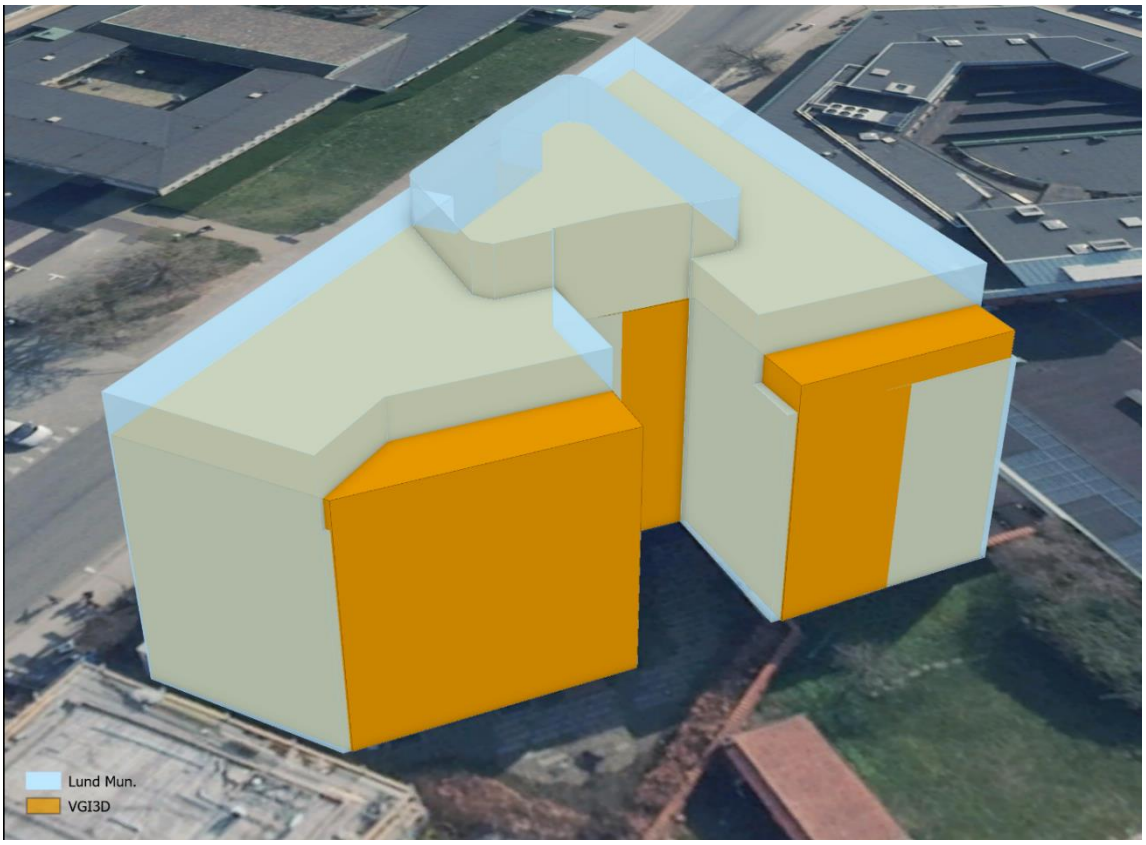

Building 6: